University of Alberta

Electric Field Gradient and its Implications in Microfabricated Post Arrays

by

Shokoufeh Kazemlou

A thesis submitted to the Faculty of Graduate Studies and Research
in partial fulfillment of the requirements for the degree of

Master of Science
in
Chemical Engineering

Department of Chemical and Materials Engineering

©Shokoufeh Kazemlou

Spring 2013
Edmonton, Alberta

Permission is hereby granted to the University of Alberta Libraries to reproduce single copies of this thesis and to lend or sell such copies for private, scholarly or scientific research purposes only. Where the thesis is converted to, or otherwise made available in digital form, the University of Alberta will advise potential users of the thesis of these terms.

The author reserves all other publication and other rights in association with the copyright in the thesis and, except as herein before provided, neither the thesis nor any substantial portion thereof may be printed or otherwise reproduced in any material form whatsoever without the author's prior written permission.

Abstract

The sources of inducing field gradients and their implications are investigated inside the microfabricated post arrays. A parametric study is conducted to understand how the posts arrangements, distance, and size change the field and field gradients. The results provide criteria where the assumption of a uniform field is valid, which can have important implications for designing microfluidic units.

The DC dielectrophoretic and electrophoretic effects on the concentration of particles through the uniformly patterned arrays of posts are also evaluated. A mathematical model is solved by using a finite element scheme in order to evaluate the electrophoretic and dielectrophoretic forces exerted on the particles. The relative magnitude of these forces is presented as a measure for predicting the fate of the particles within the microfabricated array structures. The results provide an insight into the governing particle transport mechanisms in a micro scale environment in the presence of externally applied electric fields.

Acknowledgement

I would like to take this opportunity to express my attitude to my supervisor Dr. Nazemifard who has been a steady influence throughout my M.Sc. career. She has oriented and supported me with promptness and care, and has been patient and encouraging in times of new ideas and difficulties. Above all, she made me feel a friend, which I appreciate from my heart.

I am also grateful for the funding and support provided by the Natural Sciences and Engineering Research Council of Canada (NSERC). For computing software, I thank the Integrated Nanosystems Research Facility (INRF) in the Faculty of Engineering at the University of Alberta.

Finally, I would like to thank my family for supporting me and encouraging me during my research life in Canada, and all my friends who were always next to me as close as my family.

Table of Contents

List of Tables

List of Figures

List of Symbols

a	post-to-post distance [µm]
c	particle concentration [mol.m^{-3}]
c_i	concentration of the i^{th} species [mol.m^{-3}]
C_{max}	maximum concentration in each profile [mol.m^{-3}]
d	diameter of the posts [µm]
$\bar{d}$	thickness of the device [µm]
D	particle diffusion coefficient [m^{2}.s^{-1}]
D_i	diffusivity of the i^{th} species [m^{2}.s^{-1}]
E	externally applied electric field [V.m^{-1}]
E_{rms}	amplitude (rms) of the electric field [V.m^{-1}]
F	total force exerted on the particle [N]
$\bar{F}$	Faraday constant [C.mol^{-1}]
F_{EP}	electrophoretic force [N]
F_{DEP}	dielectrophoretic force [N]
f_{CM}	Clausius-Mossotti factor
i	current density [A.m^{-2}]
I	electrical current [A]
j	particle flux [mol.m^{-2}.s^{-1}]
j_i	i^{th} species flux [mol.m^{-2}.s^{-1}]
k_b	Boltzmann constant [J.K^{-1}]
n	normal vector to the surface
N	total number of the posts in the post array structure

Pe_{EP}	peclet number based on the electrophoretic velocity
Pe_{DEP}	peclet number base on the dielectrophoretic velocity
r	particle radius [μm]
R	rate of production due to chemical reactions per unit volume [mol.m^{-3}.s^{-1}]
R_i	rate of production of i^{th} species due to chemical reactions per unit Volume [mol.m^{-3}.s^{-1}]
$\bar{R}$	gas constant [J.mol^{-1}.K^{-1}]
$Re[f_{CM}]$	real part of the Clausius-Mossotti factor
T	absolute temperature [K]
u	fluid velocity [m.s^{-1}]
U	relative velocity of a particle with respect to the liquid [m.s^{-1}]
V	voltage applied at the microchannels [V]
z_i	valence of the i^{th} species

Greek Alphabets

ε_0	permittivity of free space [F.m^{-1}]
ε_p	relative permittivity of the posts
ε_r	relative permittivity of the medium
ζ	zeta potential at the particle surface [µV]
κ^{-1}	Debye screening length [µm]
μ	dynamic viscosity of the electrolyte solution [Pa. s]
μ_e	electrophoretic mobility [m^2.V^{-1}.s^{-1}]
μ_i	mobility of the i^{th} species [m^2.V^{-1}.s^{-1}]
ρ	space charge density [C.m^{-3}]
ρ_s	surface charge [C.m^{-2}]
σ	spacing between the safe zone and the chamber walls (as the percentage of the chamber size)
σ_m	electric conductivity of the medium [S.m^{-1}]
σ_p	electric conductivity of the particle [S.m^{-1}]
υ	voltage applied at the injection channel [V]
ψ	electrical potential [V]
ψ_{in}	voltage at the inlet electrode [V]
ψ_{out}	voltage at the outlet electrode [V]

1 Introduction

1.1 Background and Overview

Microfluidics has been a rapid growing field during the last decade. One class of microfluidic devices are microfabricated post arrays (MFPAs). The ability of MFPAs to separate, manipulate, concentrate and sort particles according to size and shape is very useful in numerous fields including those involving environmental, pharmaceutical, clinical and biological applications. Miniaturized chemical and biochemical processes in microfabricated structures necessitate developing new methods of manipulating transport in micro scale environments. Since most liquid-solid interfaces bear an electrostatic charge, the application of an externally applied electric field results in the motion of the interface, a phenomenon called electrokinesis, which is one of the most frequently used methods to control the transport phenomena in microfluidics. Basic electrokinetic phenomena such as electroosmosis, electrophoresis, and dielectrophoresis, where the applied electric field and field gradients act as the driving forces, have been employed in a variety of applications such as gel electrophoresis, chromatography, pulsed field electrophoresis, capillary gel electrophoresis and insulated-based dielectrophoresis [1-9].

Particles subjected to a spatially nonuniform electric field experience electrical forces that can cause both electrophoresis and dielectrophoresis (DEP) [10-15]. Electrophoresis is the motion of the dispersed particles relative to a fluid under the influence of a spatially uniform electric field. This effect causes the particles to migrate towards the electrode of opposite charge in a DC field (Figure 1.1). Dielectrophoresis, which is caused by the presence of a nonuniform electric field, is the motion of a dielectric particle in a nonuniform electric field due to the unbalanced electrostatic forces on the particle's induced dipole [11, 14]. Dielectrophoresis has attracted much interest recently because it is an effective way to trap, manipulate, and separate particles ranging from large DNA strands to blood cells and larger particles [16-20].

This dissertation focuses on microfabricated post arrays. The electric field and field gradients, which act as driving forces to displace particles through electrophoresis and dielectrophoresis in MFPAs, are evaluated as important operational variables. Electrophoresis and dielectrophoresis are also investigated in MFPAs in order to introduce criteria that can be used to predict the particles transport mechanism. The two geometries studied in this work are presented in Figure 1.2 and Figure 1.3. Figure 1.2 shows a common microfluidic chip design including microfabricated post arrays, which has been used in several experiments such as analysis, fractionation and separation of DNA molecules [9, 21, 22]. As shown in Figure 1.2, the microchip consists of a square chamber with a packed array of micron scale posts, an injection channel, and several microchannels which surround the chamber and connect it to the electrodes, where voltages are applied. The geometry shown in Figure 1.3 is a typical design of a microfluidic channel including arrays of micron scale posts that has been used in several studies [3, 23-33] for different purposes such as dielectrophoretic concentration, passive mixing of nanoparticles, purification of DNA fragments, manipulation of bioparticles, and bioseparation.

1.2 Objectives and Scope

A precise knowledge of the parameters affecting electrokinetic transport is required in order to design a successful electrokinetic process. One of these parameters is the applied electric field. The effect of the electric field and field gradients as important operational variables on electrophoresis and dielectrophoresis in microfabricated devices have been discussed in the literature [33-35]. For some of processes, the nominal value of the field is sufficient to yield a correct calculation of the electrokinetic transport. However, when the local values of the field deviate significantly from the nominal values, the assumption of a homogeneous field is an oversimplification resulting in either failed or low efficiency processes. Large gradients of the field can also affect the mobility or trajectory of molecules by introducing dielectrophoresis. The primary objective of the work presented here is to investigate the magnitude and orientation of the electric field and the field gradients in MFPAs in order to achieve a more precise understanding of these parameters, which is required to design a successful electrokinetic process. To this end, the effect of the geometry of the microfabricated structure, the dielectric properties of the medium, and the surface charge of the interior surfaces of the microdevic on the field magnitude and orientation were evaluated. Also, a comprehensive parametric study was conducted to understand how the posts arrangements, distance, size, and surface charge change the field gradients. This study can have important implications for designing microfluidic units where a high field gradient is either favored (mixing) or not favored (separation).

After this knowledge was obtained, the effects of electrophoresis and dielectrophoresis in a MFPA were evaluated in order to identify some criteria in terms of the physical and dielectrical properties of the particles and medium, where one of the mentioned effects, i.e., electrophoresis or dielectrophoresis, is dominant. In other words, we wished to identify the particles transport mechanism under various properties of particles and medium, based on the fate of particles through uniform arrays of posts. These criteria will provide guidelines for the electrophoretic and dielectrophoretic based separation and concentration of particles in microfabricated structures and have the potential to be used for numerous chemical and biological applications. Our results show that MFPAs can be used to manipulate particles through the parameters affecting the response of the particles to the applied field, such as the zeta potential of the particles, medium permittivity and particle size, by varying the relative magnitude of the electrophoretic and dielectrophoretic flows.

1.3 Organization of the Thesis

In this chapter, the overall objectives and scope of the study have been delineated. Chapter 2, which is a literature review on this subject, provides a brief history of microfabricated structures and reviews various applications where these structures are used, and also describes the techniques which have been employed to date to control and manipulate microscopic entities inside microfabricated structures.

In Chapter 3, two series of simulations are conducted. First, the potential sources of inducing field gradients and their implications are studied. By using finite element methods, the effect of the microchip geometry, the dielectric properties of the medium, and the channels surface charge on the field magnitude and orientation are evaluated. Second, a comprehensive parametric study is conducted to determine how the posts arrangements, distance and size, and surface charge change the field gradients.

In Chapter 4, the DC dielectrophoretic and electrophoretic effects on the concentration of particles through uniformly patterned arrays of posts are evaluated. This chapter presents the characterization of the electrophoretic flow employed with DC dielectrophoresis, in order to identify the operating conditions under which one of the electrophoresis or dielectrophoresis effects is the dominant mechanism in the conformation of the particle concentration profile. Finally, Chapter 5 summarizes the key observations and conclusions from this work and provides some key recommendations for future studies in this direction.

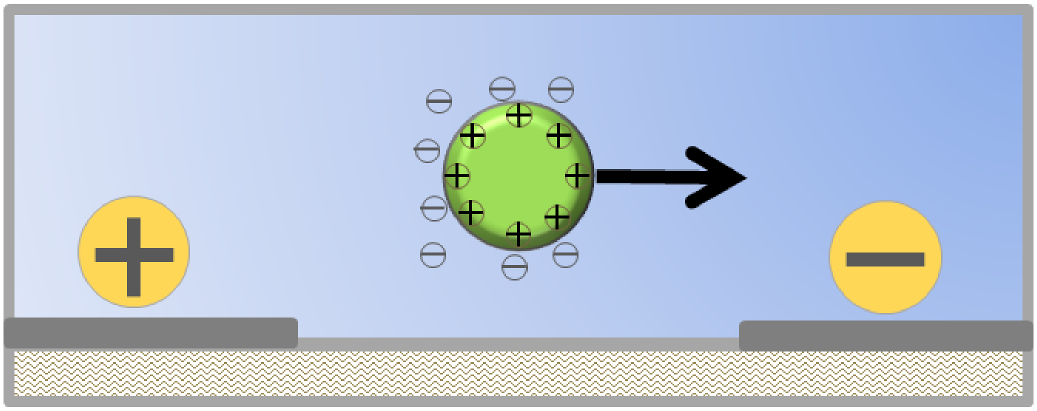

Figure 1.1 Electrophoresis – Particles migrate towards the electrode of opposite charge in a DC field

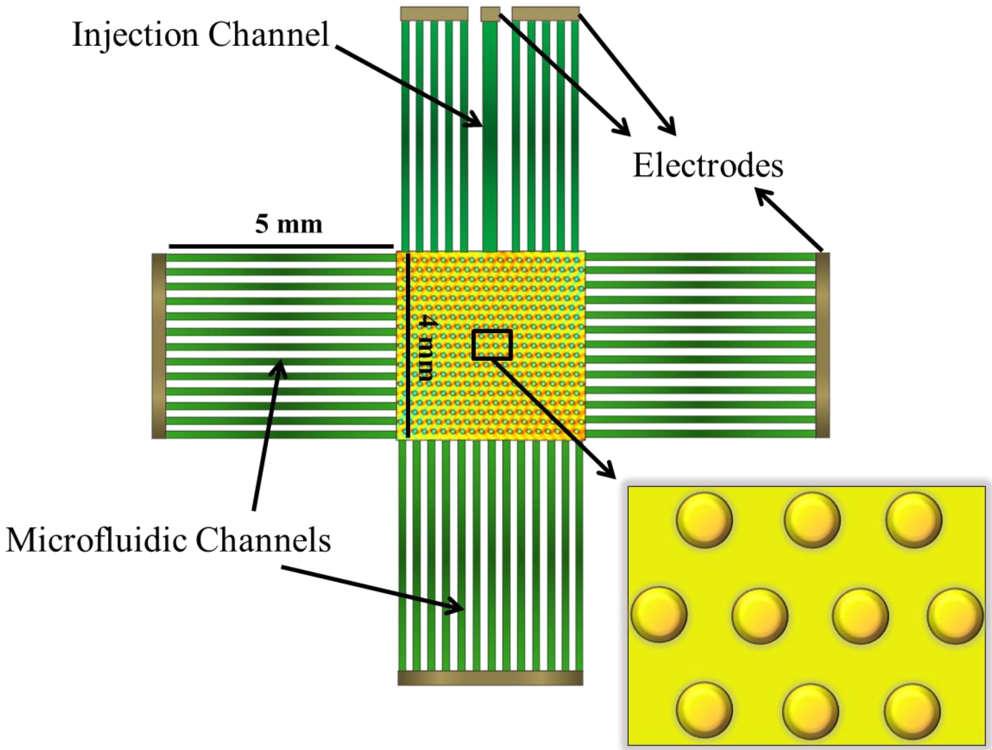

Figure 1.2 Schematic of the microfluidic chip studied in the work. The middle chamber consists of microfabricated arrays of posts. The injection channel and all the side microchannels are connected to the reservoirs where electrodes were used to apply electric voltages.

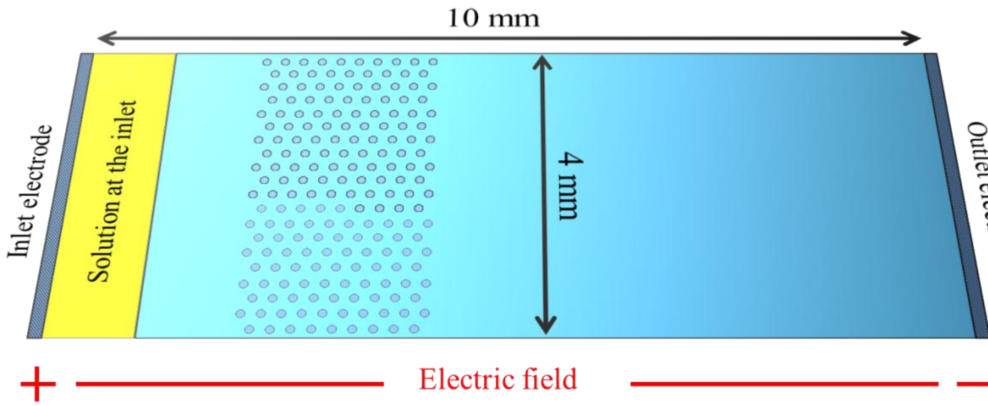

Figure 1.3 A schematic representation of the 2D microchannel studied in this work. This microchannel contains an array of posts. A suspending solution is introduced into the channel, and a DC voltage is applied to the electrodes located in the remote inlet and outlet reservoirs.

References

[1] Guttman, A., Cooke, N. *Anal. Chem.* 1991, *63*, 2038-2042.

[2] Fang, Y., Zhang, J., Hou, J., Lu, H., Dovichi, N. *Electrophoresis* 1996, *17*, 1436-1442.

[3] De Pra, M., Kok, W. T., Schoenmakers, P. J. *Journal of Chromatography a* 2008, *1184*, 560-572.

[4] Moore, A. W., Jacobson, S. C., Ramsey, J. M. *Anal. Chem.* 1995, *67*, 4184-4189.

[5] Effenhaunser, C. S., Paulus, A., Manz, A., Widmer, H. M. *Anal. Chem.* 1994, *66*, 2949-2953.

[6] Wooley, A. T., Mathies, R. A. *Proc. Natl. Acad. Sci. U. S. A.* 1994, *91*, 11348-11352.

[7] Duke, T., Austin, R., Cox, E., Chan, S. *Electrophoresis* 1996, *17*, 1075-1079.

[8] Bhattacharya, S., Chao, T., Ros, A. *Electrophoresis* 2011, *32*, 2550-2558.

[9] Chou, C. F., Tegenfeldt, J. O., Bakajin, O., et al. *Biophysical Journal* 2002, *83*, 2170-2179.

[10] Pohl, H. A. *Journal of applied Physics* 1951, *22*, 869-871.

[11] Pohl, H. A. *Dielectrophoresis*, Cambridge University Press: Cambridge 1978.

[12] Pethig, R. *Crit. Rev. Biotechnol.* 1996, *16*, 331-348.

[13] Ramos, A., Morgan, H., Green, N. G. *Appl. Phys.* 1998, *31*, 2338-2353.

[14] Jones, T. B. Electromechanics of Particles, Cambridge University Press: New York 1995.

[15] Pysher, M. D., Hayes, M. A. *Analytical Chemistry* 2007, *79*, 4552-4557.

[16] Gascoyne, P., Huang, Y., Pethig, R., Vykoukal, J., Becker, F. *Meas Sci Technol* 1992, *3*, 439-445.

[17] Gascoyne, P., Huang, Y., Wang, X., Becker, F. *Biophys. J.* 1994, *66*, A238-A238.

[18] Gascoyne, P., Huang, Y., Vykoukal, J., Becker, F., Wang, X. *Biophys. J.* 1997, *72*, WPME2-WPME2.

[19] Pethig, R., Huang, Y., Wang, X., Burt, J. *Journal of Physics D-Applied Physics* 1992, *25*, 881-888.

[20] Pethig, R., Markx, G. *Trends Biotechnol.* 1997, *15*, 426-432.

[21] Huang, L., Tegenfeldt, J., Kraeft, J., Sturm, J. *et al*. *Nat. Biotechnol.* 2002, *20*, 1048-1051.

[22] Zeng, Y., He, M., Harrison, D. J. *Angewandte Chemie-International Edition* 2008, *47*, 6388-6391.

[23] Jeon, W., Shin, C. B. *Chemical Engineering Journal* 2009, *152*, 575-582.

[24] Martinez-Lopez, J. I., Moncada-Hernandez, H., Baylon-Cardiel, J. L., et al. *Analytical and Bioanalytical Chemistry* 2009, *394*, 293-302.

[25] Moncada-Hernandez, H., Baylon-Cardiel, J. L., Perez-Gonzalez, V. H., et al. *Electrophoresis* 2011, *32*, 2502-2511.

[26] Cummings, E. B. *IEEE Engineering in Medicine and Biology Magazine* 2003, *22*, 75-84.

[27] Nakano, A., Camacho-Alanis, F., Chao, T., et al. *Biomicrofluidics* 2012, *6*, 034108.

[28] Cummings, E., Singh, A. *Anal. Chem.* 2003, *75*, 4724-4731.

[29] Cummings, E. B., Singh, A. K. *Analytical Chemistry* 2003, *75*, 4724-4731.

[30] Xu, Y. C., Vaidya, B., Patel, A. B., et al. *Analytical Chemistry* 2003, *75*, 2975-2984.

[31] Kuo, C., Shiu, J., Wei, K. H., et al. *Journal of Chromatography a* 2007, *1162*, 175-179.

[32] Shiu, J., Whang, W., Chen, P. *Journal of Chromatography a* 2008, *1206*, 72-76.

[33] Chen, G. D., Fachin, F., Fernandez-Suarez, M., Wardle, B. L., Toner, M. *Small* 2011, *7*, 1061-1067.

[34] Dorfman, K. D. *Reviews of Modern Physics* 2010, *82*, 2903-2947.

[35] Oh, D., Cheong, I. C., Lee, H. G., Eo, S. K., Kang, S. H. *Bulletin of the Korean Chemical Society* 2010, *31*, 1902-1906.

2 Literature review

2.1 Microfluidics and Microfabrication

In the early 1990s Microfluidics devices were developed and fabricated in silicon and glass by etching techniques and photolithography [1]. A detailed review of the history and development of microfluidics is conducted by Zimmerman [2] presenting specific applications of microfluidics including electrokinetic flow and electrokinetic bioanalytical systems. There has been an increasing trend towards the analytical chip based microdevices after the introduction of the concept of micro total analysis systems (μ-TAS) in 1989. One class of microfluidic devices are microfabricated arrays. Historically the earliest microfabrication processes were used for integrated circuit fabrication. Microfabrication technologies originated from the microelectronics industry. The devices are usually made on silicon wafers, glass, plastics, PDMS, etc. [3]. The focus of this study is not to discuss how the microfabricated devices are constructed, but it can easily be obtained in standard text on microfabrication [4].

Recent developments in micro scale fabrication techniques allow for innovative experimentation of the role of microfluidic systems in various fields including biotechnology, engineering, medicine, clinical and biochemical processing for different applications such as separation [5-10], detection [11-13], mixing [14], purification [15-17], sequencing [18], fractionation [19-22] and sorting [23-26]. The methods of fabrication and the application of microfabricated devices in biotechnology and biochemical processing have been discussed in a work by Chavon and Guttman [27]. In recent years there has been increasing progress in applying microfabrication and soft lithographic techniques in the separation of biomolecules and in studying various biosystems [24]. DNA electrophoresis which is often synonym with DNA separation is one of the most significant applications of microfabricated devices and has been the subject of numerous studies [5, 6, 9, 10] in the past two decades.

2.2 Microfabricated Post Arrays

Microfabricated post arrays (MFPA) have been evaluated in numerous studies [10, 25, 28-33] for various applications including separation, mixing and manipulation of micron scale entities through different electrokinetic techniques. Several examples of analytical chip based microsystems, including microarray systems have been detailed in reviews by Manz and Becker [34], Sanders and Manz [35], and Kricka [36]. DNA electrophoresis in microlithographic post arrays, first established by Volkmuth and Austin [6], is comprehensively discussed in the recent review by Dorfman [5] who synthesized the theoretical models, simulation results, and experimental data for DNA electrophoresis in micro/nanofabricated devices appearing since the seminal paper by Volkmuth and Austin [6].

In 1992, Volkmuth and Austin [37] used a post array to fractionate large DNA molecules which the gel matrix was not capable to fractionate. Their post array structure extended the limits of conventional DC electrophoresis in agarose gel.

Duke et al. [38] also employed a microfabricated post array to separate DNA molecules through pulsed field electrophoresis. They stated that the dynamic of DNA undergoing pulsed field electrophoresis is more straightforward in the microfabricated array than in a gel.

Cummings and Singh [31] investigated different regimes for particle transport in a microchip containing arrays of insulating posts when a DC field is applied. They showed that the post array have the potential to produce highly concentrated or rarefied streams of particles through reinforcing the dielectrophoretic movement of the particles. Ros et al. [39] also employed post arrays fabricated at the intersection of cross-shaped microchannels for the docking of single cells.

The first geometry studied in this work (shown in Figure 1.2) is a common microfluidic chip design that has been used in several experiments [9, 10, 33, 40]. Zeng et al. [33] have employed a similar geometry to obtain high-throughput continuous DNA fractionation. They have demonstrated a general microfluidic approach for patterning large scale colloidal nanoarrays into microdevices. Their studies on the effects of pulsed electric field and pore size provided a clear guidance which can be useful for choosing proper field conditions to sort DNA samples.

Huang et al. [9] also used the similar geometry for DNA separation, considering the fact that the sizes of DNA molecules can be distinguished by measuring their migration speeds under electric fields. They replaced the sieving matrix with an array of microposts in the microfabricated chip, which can achieve separation in a few seconds in the 100 kb range [41]. Their microchip geometry similarly consisted of an array of micronscale posts as the sieving matrix, and relied on integrated microfluidic channels to spatially tune uniform electric fields over the matrix. The second geometry evaluated in this study (as shown in Figure 1.3), is a typical design of microfluidic channel including arrays of micron scale post that has been used in several studies [14, 15, 42-46]. Martinez-Lopez et al. [42] used a similar geometry for characterization of electrokinetic mobility of the particles to improve dielectrophoretic concentration. Their measurements established that optimal conditions for dielectrophoretic trapping, when electroosmosis is present, are low pH and high conductivity for the suspending medium. Davalos et al. [47] employed the similar geometry to evaluate the performance of polymer based dielectrophoresis device for the selective trapping and concentration of biological and inert particles in an aqueous sample. Moncada-Hernandez et al. [43] studied the dielectrophoretic behaviour of microorganisms through mathematical modeling and experimentation in a similar geometry.

2.3 Electric Field in Microfabricated Devices

Physical manipulation of biochemical species is often carried out using acoustic, electrical, magnetic, or optical forces. These methods permit diverse particle manipulations with minimal mechanical contact between particles and device structures, and they are mostly applied to microfluidic platforms where contact free manipulation of particles is required to reduce negative effects such as clogging of device channels. In such applications, deploying these methods increases accuracy, automation, and throughput to transport, analyze, sort, or modify individual species. [48-51].

Electro manipulation refers to diverse uses of electric fields to manipulate micrometer sized objects [52]. This method has been used for decades to drive flow, move analytes, and separate chemical and biochemical species in micrometer sized channels where dimensions of electrokinetically driven flows inside channels are comparable to the electric double layer.[53-59]. Electrical manipulation of biochemical species is achieved using AC, DC, or pulsed electric fields for various applications that are summarized in Table 2.1 [42, 60-66].

More complete discussion of electrical manipulation and different types of applied electric field and their impact on biochemical species can be found in the text by Zimmermann and Neil [52]. Different methods of applying electric fields for on-chip manipulation and assembly of colloidal particles have been reviewed by Velev and Bhatt in [40]. AC polarization forces are mostly used to induce translation, rotation, and deformation of cells, and pulsed fields to disrupt sub cellular structures. Overviews on the principles and interrelations of different electrical manipulation methods are described in [67-71].

Control of electric fields plays a critical role in the accurate manipulation of particles. For example, electric fields must be maintained uniform across a two dimensional area where the pulsed field gel electrophoresis (PFGE) are used to separate DNA of different sizes. Huang et al. [41] presented a novel method for generating tunable uniform electric fields over large microfluidic arrays in two dimensions, and its application to a microfabricated device that separates genomic DNA. A novel method was presented in [48] to generate tunable uniform electric fields across large two dimensional arrays. The application of the method to separate genomic DNA in microfabricated structures was also presented. Figure 2.1 illustrates three methods to create tunable fields in a two dimensional area. The current injection method (Figure 2.1 c), was introduced by Huang et al. [41].

A microfabricated DNA prism device was reported by Huang et al. [30] that continuously sorts large DNA molecules (61 kilobase pair to 209 kb) according to size in 15 seconds. The geometry of the device is shown in Figure 2.2. DNA was continuously injected into the post array using alternating electric pulses of different strengths and durations. Then DNA fragments were separated as they flow through the array, and the sorted DNA in microfluidic channels were collected for further downstream analysis. The uniform electric fields that were generated by microchannels across the entire array were necessary to shape straight bands of injected molecules.

As mentioned by Cummings and Singh in [77], tuning field strength can vary the relative magnitudes of electrokinetic flow and DEP, that causes microfabricated devices become electrically biased to manipulate particles selectively. It is shown that post shapes can be easily contoured to control electric field gradients and, hence, DEP behavior. In [51], the effective conductance of the array is defined as the total current through the array to the applied electric field. Cummings [51] demonstrated that the effective conductance is a function of post shape and size. In [29], the electric field gradients are measured as a function of the post size and geometry. For this purpose, an electric field is applied across a microchannel containing insulating posts.

Detailed knowledge of electric field distribution is required to proper use of the microfabricated post arrays. Accurate modeling and simulations need to be carried out in order to avoid mistakes such as unintentional particle traps and escapes, to develop design details, and ultimately to optimize device performance.

2.4 Electrophoresis

The history of electrophoresis begins with the pioneering work of the Swedish biochemist, Arne Tiselius. He published his first paper on electrophoresis in 1937 [72]. New separation processes and chemical analysis techniques based on electrophoresis continue to be developed into the 21st century [73, 74]. The term electrophoresis was coined from the Greek word “phoresis”, which means ‘being carried’. Thus, the electrophoresis means being carried by an electrical field [72].

Electrophoresis which is the ability to drive the particles towards an oppositely charged electrode in an applied electric field, can be used for the particle separation, concentration, deposition, or colloidal crystallization [40, 75-78]. Electrophoresis in microchannels is characterized by the dominant presence of the electrical double layer (EDL) that is formed at the interface between a solid and an electrolyte. Smoluchowski developed the most known theory of electrophoresis in 1903 [79]

$$\mu_e = \frac{\varepsilon_r \varepsilon_0 \zeta}{\mu}$$

Where ε_r is the relative permittivity of the dispersion medium, ε_0 is the permittivity of free space, μ is the dynamic viscosity of the dispersion medium, and ζ is the zeta potential of the particle. The Smoluchowski theory works for any shape of dispersed particles at any concentration. This theory is valid only for sufficiently thin double layer, when particle radius, r, is much greater than the Debye length ($\kappa r >> 1$), which is the considered condition in this study.

Different methods of electrophoresis have been developed since the 1950s, including zone electrophoresis (ZE), gel electrophoresis (GE), and capillary electrophoresis (CE).

Capillary zone electrophoresis which has attracted the main attention among the various electrophoretic methods, employs narrow bore capillaries to perform electrophoretic separations. Since capillary cross sectional dimensions have the same scale of the typical microfluidic channels, miniaturization efforts have focused on scale down of capillary electrophoresis technologies [80]. Microchip electrophoresis is an analytical technique resulted from miniaturization of capillary electrophoresis to a planar microfabricated separation device. Recently, microchip electrophoresis has risen above all of the other electrophoresis methods because it maintains all of the advantages of CE and exhibits advanced separation efficiency over a short analysis time [76, 81, 82].

The electrophoresis has been also applied in microfabricated post arrays for particle manipulation. Bakajin et al. [83] introduced the transverse pulsed field electrophoresis in a hexagonal array of micron scale posts, in order to separate large DNA molecules a few seconds. Their device consisted of a microfabricated sieving matrix and a narrow constriction for sample concentration. Pulsed fields were created with two pairs of electrodes connecting to the edge of the array. However, it had limitations including distortion of the electric field by the electrodes, and limited amount of material that can be analyzed. Huang et al. [30] removed these limitations by reporting a new microchip geometry including arrays of micron scale posts, for electrophoresis of large DNA molecules. Their microfluidic device consisted of a hexagonally packed array of micron scale posts, sample injection channel, sample extraction channel, and structures for shaping uniform electric fields. They injected DNA continuously into the post array using electric field pulses, and separated DNA fragments as they followed through the array.

2.5 Dielectrophoresis

DEP is a well-known particle manipulation technique that takes advantage of the interaction of polarizable matter with nonuniform electric fields. The most important requirement for this technique is the implementation of an electric field gradient that induces a dipolar moment on the particle of interest. The technique was first described by Pohl in the 1950s [84]. The great potential of the technique to selectively manipulate targeted particles was well realized then but it was not until the establishment of miniaturization techniques in the 1990s that DEP became a popular research field. The use of microfabrication techniques allowed for the positioning of electrodes very close to each other, by tens of micrometers, and therefore the use of practical voltages, tens of volts, instead of thousands of volts required in the initial experiments where electrodes were separated by centimeters. The 1990s saw an explosion of DEP publications, mainly from the groups of Pethig, Gascoyne, Fuhr, and Morgan and Green who used metal microelectrodes to sort a wide variety of cells as reviewed a number of times before [85-87]. The development of microfluidics also allowed for the creation of better devices for flow management and better understanding of the interaction between hydrodynamic and electrokinetic forces. Starting in the 2000s, alternative techniques started to arise to overcome common problems in metal electrode DEP, such as electrode fouling, and/or to increase the throughput of the system. Insulator based DEP (iDEP) and light induced DEP (LIDEP) are the most significant examples.

There has been a significant increase in the number of DEP publications over the past decade. A search of databases generates details of nearly 2000 publications (excluding conference reports and patents) in this field of study over the past 10 years [87]. The papers cover various aspects of the theory and technology. Published applications of DEP are directed toward areas such as biosensors, cell therapeutics, drug discovery, medical diagnostics, microfluidics, nanoassembly, and particle filtration. Most publications on DEP quote an expression for the time-average DEP force (acting on a spherical particle) of the form [87]

$$F_{DEP} = 2\pi\varepsilon_r \varepsilon_0 r^3 f_{CM} (\nabla E_{rms}{}^2)$$

Where r is the particle radius, ε_r is the relative permittivity of the medium, ε_0 is the permittivity of free space, f_{CM} is the Clausius-Mossotti factor related to the effective polarizability of the particle, E_{rms} is the amplitude (rms) of the electric field, and ∇ represents the gradient operator.

In order to move particles of the order of 1–10 µm in diameter, a field of 10^4-10^5 $V.m^{-1}$ is required [88]. Early studies of DEP effects were undertaken using large electrode structures and high voltages [66]. Recent works [89-94] have demonstrated that DEP can be used to manipulate particles smaller than 1 µm in diameter. Pohl [66] showed that excessively large electrical field gradients would be required to move a particle of, for example, 500 nm diameter. Particles such as plant and animal viruses, latex beads, DNA, and macromolecules can be moved by DEP [89-91, 93].

A recent review by Martinez Duarte [95] has discussed how different fabrication techniques can improve the development of practical DEP devices to be used in different settings such as clinical cell sorting and infection diagnosis, industrial food safety, and enrichment of particle populations for drug development.

A comprehensive study on DEP theory and applications is conducted by Pething [87], and Gascoyne has studied the application of dielectrophoresis to particle separation and fractionation in his review [96]. A number of studies have focused on the application of DEP for concentration, separation, transport, and identification of bacteria [97-101]. The majority of DEP studies reported in the literature employ AC electric fields and closely spaced electrode arrays to produce the nonuniform fields. However, microelectrode array based DEP systems generally face performance limiting issues such as electrode fouling. An alternative to electrode based DEP is called insulator based DEP (iDEP). Cummings and Singh [31, 102] introduced the concept and initial characterization of an iDEP device consisting of an array of insulating posts in a microchannel. In their experiments a DC electric field was applied across this microchannel. The insulating posts created electric field intensity gradients. Cummings and Singh [2,17,18] successfully demonstrated dielectrophoretic manipulation and trapping of 200 nm fluorescent polystyrene particles. They demonstrated iDEP with polystyrene particles using DC electric fields [31, 102]. Chou et al. [103] demonstrated iDEP trapping of DNA molecules using insulating structures and AC electric fields. Zhou et al. [104] and Suehiro et al. [105] used a channel filled with insulating glass beads and AC electric fields for separating and concentrating yeast cells in water. In their system, the direction of the water flow was normal to the applied electric field. Lapizco-Encinas et al. [29] demonstrated selective iDEP trapping of polystyrene particles, live E. coli, and dead E. coli in arrays of insulating posts using DC electric fields.

2.6 DEP and EP Relative Magnitude

Particle flows show a different behavior with respect to the relative magnitude of electrokinetic (EK) and dielectrophoretic forces when EK, DEP, and particle diffusion occur together in a microchannel. The flows can be classified into three types [31]: EK flow, streaming DEP flow, and trapping DEP flow. The EK flow is produced where particle transports are considerably affected by EK and diffusion because the effect of DEP is weak. As a result, the particles move almost parallel to electric field lines. In a streaming DEP flow, occurring at moderate relative magnitudes of DEP and EK forces, particles migrate along particular streamlines because the effect of DEP is balanced with the effects of EK and diffusion. Finally, a trapping DEP flow occurs when the relative magnitude of DEP to EK forces is high and the flow is dominated by DEP. Cummings and Singh [31] introduced these three regimes in microfabricated arrays of insulating posts. They demonstrated that streaming dielectrophoresis can be coherently reinforced within a patterned array of posts to produce highly concentrated or rarefied streams of particles. They also developed simple mathematical models and continuum simulations based on ideal electrokinetic flow and dielectrophoresis that have the potential to be used to design novel dielectrophoretic concentrators and sorters. Kwon et al. [106] investigated the EK and DEP forces exerted on particles in a microfabricated post array, employing numerical simulations and proposed an improved geometry to increase particle transport in EK flow regime. They classified the three flow types by electric field intensity: low electric field (EK flow), moderate electric field (streaming DEP), and high electric field (trapping DEP), and distinguished the flow types by dimensionless variables that were derived by considering the directions of particle flux and electric field. Their work describes the theoretical background of EK and DEP discussing the criteria for characterizing particle flow in terms of the applied electric field and its intensity when it is heterogeneous.

Cummings [44] introduced streaming dielectrophoresis as a novel flow regime for device development that can be coherently reinforced within a patterned array to produce strong particle depletion and enhancement effects. Kwon et al. [106] developed a numerical program to predict EK and DEP in a microchannel consisting post array, and presented an improved microchannel geometry with a circular post array, for enhanced particle transports across EK streamline for a given power dissipation. They indicated that a low electric field might be used to obtain the desired DEP effects through a smart design of a microfabricated post array with numerical simulations.

Moncada-Hernandez et al. [43] analyzed and compared the magnitude of electrokinetic and dielectroporesis mobilities and established a condition in terms of applied electric field, for dielectrophoretic trapping for the cells in a microfabricated array of cylindrical posts.

Davalos et al. [47] carried out simulations of trapping regions in a post array by analysis of the ratio between the gradient of E^2 and the magnitude of the local electric field. Martinez-Lopez et al. [42] evaluated dielectrophoretic and electrokinetic forces exerted on the particles in a microchannel with cylindrical post array. They characterized electrokinetic under the operating conditions employed for DEP separations when DC electric field was employed, in order to improve and optimize insulator based DEP separation processes. Their study identified the operating conditions in forms of the PH and conductivity of the suspending medium, under which the electrokinetic force is the lowest, enhancing dielectrophoretic trapping and concentration. Lapizco Encinas et al. [107] employed DEP trapping regime to selectively separate and concentrate live bacteria in a microchannel containing an array of posts, employing different intensities of the applied electric field. They introduced different threshold applied electric fields required to trap each bacteria species.

To the best of my knowledge, no research has been conducted to evaluate the relative magnitude of diffusion, electrokinesis, and dielectrophoresis forces in a microfabricated post array, in order to predict the governing mechanism for particle transport.

Table 2.1 Different types of electrical particle manipulation [51]

Name	Abbr.	Applied Field	Effect	Reference
Dielectrophoresis	DEP	AC and DC	Displacement	[66]
Electrophoresis	EP	DC	Displacement	[64, 71]
Electro-rotation	ER	Oscillating	Rotation	[60, 65]
Electro-deformation	ED	Oscillating	Deformation	[61]
Electro-disruption	EDIS	Pulsed	Disruption of subcellular structures	[62]
Electro-destruction	EDES	Pulsed	Lysis	[63]

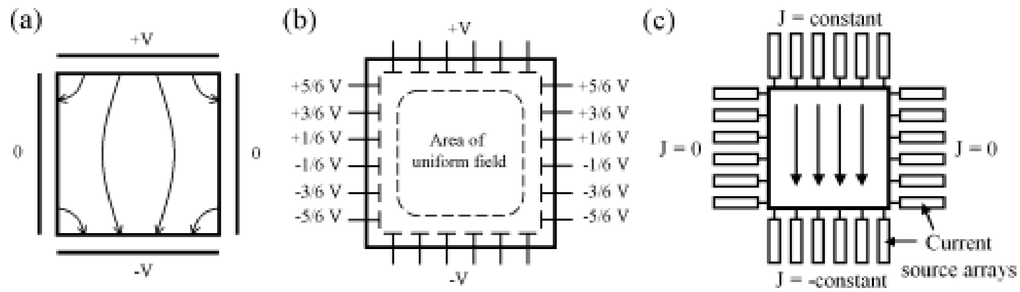

Figure 2.1 (a) Highly nonuniform field generated by four electrodes. (b) Contour clamped homogeneous electric field (CHEF) method, used in conventional PFGE apparatuses. (c) Current injection method [41].

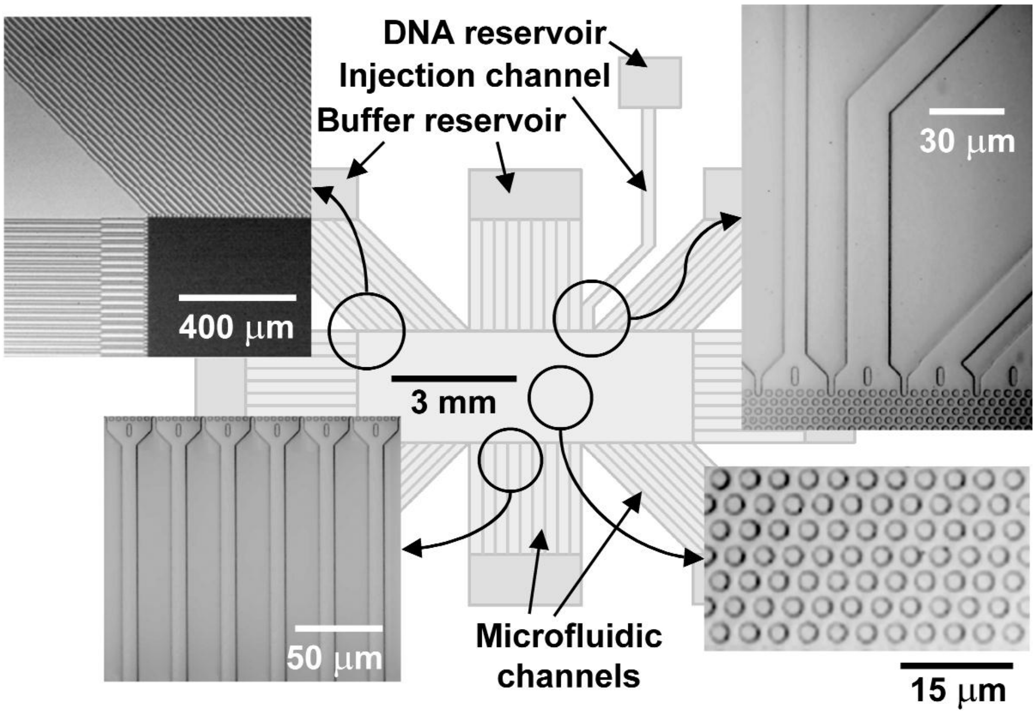

Figure 2.2 Structure of the microfabricated device illustrating the sieving matrix integrated with the microfluidic channels. The many microfluidic channels connecting to buffer reservoirs produce uniform electric fields over the sieving matrix by acting as electric current injectors [30].

References

[1] Ouellette, J. *The Industrial Physicist* 2003, 14-17.

[2] Zimmerman, William B. J. (Ed.). *Microfluidics: History, Theory and Applications*, CISM International Centre for Mechanical Sciences 2006.

[3] Andersson, H., van den Berg, A. *Sensors and Actuators B-Chemical* 2003, *92*, 315-325.

[4] Campbell, S. A. *The Science and Technology of Microelectronic Fabrication*, Oxford, Oxford University Press 2007.

[5] Dorfman, K. D. *Reviews of Modern Physics* 2010, *82*, 2903-2947.

[6] Volkmuth, W., Austin, R. *Nature* 1992, *358*, 600-602.

[7] Becker, M., Marggraf, U., Janasek, D. *Journal of Chromatography a* 2009, *1216*, 8265-8269.

[8] Costa, R., Mogensen, K., Kutter, J. *Lab on a Chip* 2005, *5*, 1310-1314.

[9] Huang, L., Tegenfeldt, J., Sturm, J., Austin, R., Cox, E. *A DNA prism: Physical principles for optimizing a microfabricated DNA separation device* 2002.

[10] Ou, J., Joswiak, M. N., Carpenter, S. J., Dorfman, K. D. *Journal of Vacuum Science & Technology a* 2011, *29*.

[11] Kang, C. M., Joo, S., Bae, J. H., Kirn, Y. *et al*. *Anal. Chem.* 2012, *84*, 901-907.

[12] Munro, N., Snow, K., Kant, E., Landers, J. *Clin. Chem.* 1999, *45*, 1906-1917.

[13] Pepper, J., Noring, R., Klempner, M., Cunningham, B. *et al*. *Sensors and Actuators B-Chemical* 2003, *96*, 565-575.

[14] Jeon, W., Shin, C. B. *Chemical Engineering Journal* 2009, *152*, 575-582.

[15] Xu, Y. C., Vaidya, B., Patel, A. B., et al. *Analytical Chemistry* 2003, *75*, 2975-2984.

[16] Hoffstetterkuhn, S., Kuhn, R., Wagner, H. *Electrophoresis* 1990, *11*, 304-309.

[17] Cady, N., Stelick, S., Batt, C. *Biosens. Bioelectron.* 2003, *19*, 59-66.

[18] Carrilho, E. *Electrophoresis* 2000, *21*, 55-65.

[19] Bakajin, O., Duke, T., Chou, C., Tegenfeldt, J. *et al*. *Biological Physics* 1999, *487*, 243-248.

[20] Lu, H., Gaudet, S., Schmidt, M., Jensen, K. *Anal. Chem.* 2004, *76*, 5705-5712.

[21] Bakajin, O., Duke, T., Chou, C., Chan, S. *et al*. *Biophys. J.* 2000, *78*, 266A-266A.

[22] Bakajin, O., Duke, T., Chou, C., Tegenfeldt, J. *et al*. *Biophys. J.* 1999, *76*, A398-A398.

[23] Giang, U. T., King, M. R., DeLouise, L. A. *Journal of Bionic Engineering* 2008, *5*, 308-316.

[24] Chou, C., Austin, R., Bakajin, O., Tegenfeldt, J. *et al*. *Electrophoresis* 2000, *21*, 81-90.

[25] Castelino, J., Austin, R. *Biophys. J.* 2000, *78*, 254A-254A.

[26] Chou, H., Spence, C., Scherer, A., Quake, S. *Micro- and Nanofabricated Structures and Devices for Biomedical Environmental Applications* 1998, *3258*, 181-187.

[27] Chovan, T., Guttman, A. *Trends Biotechnol.* 2002, *20*, 116-122.

[28] Hunt, T., Lee, H., Westervelt, R. *Appl. Phys. Lett.* 2004, *85*, 6421-6423.

[29] Lapizco-Encinas, B., Simmons, B., Cummings, E., Fintschenko, Y. *Anal. Chem.* 2004, *76*, 1571-1579.

[30] Huang, L., Tegenfeldt, J., Kraeft, J., Sturm, J. *et al*. *Nat. Biotechnol.* 2002, *20*, 1048-1051.

[31] Cummings, E. B., Singh, A. K. *Analytical Chemistry* 2003, *75*, 4724-4731.

[32] Bhattacharya, S., Chao, T., Ros, A. *Electrophoresis* 2011, *32*, 2550-2558.

[33] Zeng, Y., He, M., Harrison, D. J. *Angewandte Chemie-International Edition* 2008, *47*, 6388-6391.

[34] Manz, A., Becker, H. *Microsystem Technology in Chemistry and Life Science*, Berllin, Springer Verlag 1998.

[35] Sanders, G., Manz, A. *Trac-Trends in Analytical Chemistry* 2000, *19*, 364-378.

[36] Kricka, L. *Clin. Chem.* 1998, *44*, 2008-2014.

[37] Volkmuth, W., Austin, R. *Nature* 1992, *358*, 600-602.

[38] Duke, T., Austin, R., Cox, E., Chan, S. *Electrophoresis* 1996, *17*, 1075-1079.

[39] Ros, A., Hellmich, W., Regtmeier, J., Duong, T. T., Anselmetti, D. *Electrophoresis* 2006, *27*, 2651-2658.

[40] Velev, O. D., Bhatt, K. H. *Soft Matter* 2006, *2,* 738-750.

[41] Huang, L. R., Tegenfeldt, J. O., et al. *Technical Digest of International Electron Devices Meeting* 2001, 363-366.

[42] Martinez-Lopez, J. I., Moncada-Hernandez, H., Baylon-Cardiel, J. L., et al. *Analytical and Bioanalytical Chemistry* 2009, *394*, 293-302.

[43] Moncada-Hernandez, H., Baylon-Cardiel, J. L., Perez-Gonzalez, V. H., et al. *Electrophoresis* 2011, *32*, 2502-2511.

[44] Cummings, E. B. *IEEE Engineering in Medicine and Biology Magazine* 2003, *22*, 75-84.

[45] Kuo, C., Shiu, J., Wei, K. H., et al. *Journal of Chromatography a* 2007, *1162*, 175-179.

[46] Shiu, J., Whang, W., Chen, P. *Journal of Chromatography a* 2008, *1206*, 72-76.

[47] Davalos, R. V., McGraw, G. J., Wallow, T. I., Morales, A. M. *et al*. *Analytical and Bioanalytical Chemistry* 2008, *390*, 847-855.

[48] Feng, X., Du, W., Luo, Q., Liu, B. *Anal. Chim. Acta* 2009, *650*, 83-97.

[49] Nilsson, J., Evander, M., Hammarstrom, B., Laurell, T. *Anal. Chim. Acta* 2009, *649*, 141-157.

[50] Wlodkowic, D., Cooper, J. M. *Analytical and Bioanalytical Chemistry* 2010, *398*, 193-209.

[51] MacQueen, L. A., Thibault, M., Buschmann, M. D., Wertheimer, M. R. *IEEE Trans. Dielectr. Electr. Insul.* 2012, *19*, 1261-1268.

[52] Zimmermann, U., Neil, G. A. *Electromanipulation of cells*, Boca Raton, Fla., USA, CRC Press 1996.

[53] Burgreen, D., Nakache, F. *J. Phys. Chem.* 1964, *68*, 1084-&.

[54] Hildreth, D. *J. Phys. Chem.* 1970, *74*, 2006-&.

[55] Rice, C., Whitehea.R. *J. Phys. Chem.* 1965, *69*, 4017-&.

[56] Levine, S., Marriott, J., Neale, G., Epstein, N. *J. Colloid Interface Sci.* 1975, *52*, 136-149.

[57] Levine, S., Marriott, J., ROBINSON, K. *Journal of the Chemical Society-Faraday Transactions Ii* 1975, *71*, 1-11.

[58] Zheng, Z., Hansford, D., Conlisk, A. *Electrophoresis* 2003, *24*, 3006-3017.

[59] Tessier, F., Slater, G. *Electrophoresis* 2006, *27*, 686-693.

[60] Arnold, W., Zimmermann, U. *J. Electrostatics* 1988, *21*, 151-191.

[61] Engelhardt, H., Sackmann, E. *Biophys. J.* 1988, *54*, 495-508.

[62] Beebe, S., White, J., Blackmore, P., Deng, Y. *et al*. *DNA Cell Biol.* 2003, *22*, 785-796.

[63] SALE, A., HAMILTON, W. *Biochim. Biophys. Acta* 1968, *163*, 37-&.

[64] Weinberger, R. *Practical Capillary Electrophoresis*, Chappaqua, New York, U.S.A., CE Technologies 2000.

[65] Jones, T. B. Electromechanics of Particles, Cambridge University Press: New York 1995.

[66] Pohl, H. A. *Dielectrophoresis*, Cambridge University Press: Cambridge 1978.

[67] Jordan, C. A., Neumann, E., Sowers, A. E. *Electroporation and Electrofusion in Cell Biology*, New York, Plenum Press 1989.

[68] Delgado, A. V. *Interfacial Electrokinetics and Electrophoresis*, New York, USA, Marcel Dekker, Inc. 2002.

[69] Hughes, M. P. *Nanoelectromechanics in Engineering and Biology*, Boca Raton, FL, USA, CRC Press 2003.

[70] Nickoloff, J. A. *Animal Cell Electroporation and Electrofusion Protocols*, Totowa, N.J., USA, Humana Press 1995.

[71] Morgan, H., Green, N. G. *AC Electrokinetics: Colloids and Nanoparticles*, Research Studies Pr 2003.

[72] http://www.monzir-pal.net/Bioseparation/Lectures/L31.pdf.

[73] Vesterberg, O. *J. Chromatogr.* 1989*, 480*, 3-19.

[74] http://en.wikipedia.org/wiki/History_of_electrophoresis.

[75] Fonslow, B. R., Bowser, M. T. *Anal. Chem.* 2008*, 80*, 3182-3189.

[76] Oh, D., Cheong, I. C., Lee, H. G., Eo, S. K., Kang, S. H. *Bulletin of the Korean Chemical Society* 2010*, 31*, 1902-1906.

[77] Tran, N. T., Ayed, I., Pallandre, A., Taverna, M. *Electrophoresis* 2010*, 31*, 147-173.

[78] Giersig, M., Mulvaney, P. *Langmuir* 1993*, 9*, 3408-3413.

[79] Smoluchowski, M. V. *Bull, Int. Acad. Sci. Cracovie* 1903*, 8*, 182-200.

[80] http://www.aesociety.org/areas/microchip_electrophoresis.php.

[81] Kim, D., Kang, S. *Journal of Chromatography a* 2005*, 1064*, 121-127.

[82] Lee, M., Yoon, D., Jeon, J., Eo, S. K., Kang, S. H. *Bulletin of the Korean Chemical Society* 2009*, 30*, 2655-2660.

[83] Bakajin, O., Duke, T., Tegenfeldt, J., Chou, C. *et al*. *Anal. Chem.* 2001*, 73*, 6053-6056.

[84] Pohl, H. A. *Journal of applied Physics* 1951*, 22*, 869-871.

[85] Gascoyne, P., Vykoukal, J. *Proc IEEE* 2004*, 92*, 22-42.

[86] Pohl, h., Hawk, I. *Science* 1966*, 152*, 647-&.

[87] Pethig, R. *Biomicrofluidics* 2010*, 4*, 022811.

[88] Ramos, A., Morgan, H., Green, N. G. *Appl. Phys.* 1998*, 31*, 2338-2353.

[89] Muller, T., Fiedler, S., Schnelle, T., Ludwig, K. *et al*. *Biotechnol. Tech.* 1996*, 10*, 221-226.

[90] Muller, T., Gerardino, A., Schnelle, T., Shirley, S. *et al*. *Journal of Physics D-Applied Physics* 1996, *29*, 340-349.

[91] Washizu, M., Suzuki, S., Kurosawa, O., Nishizaka, T., Shinohara, T. *IEEE Trans. Ind. Appl.* 1994, *30*, 835-843.

[92] Green, N., Morgan, H., Milner, J. *J. Biochem. Biophys. Methods* 1997, *35*, 89-102.

[93] Green, N., Morgan, H. *Journal of Physics D-Applied Physics* 1997, *30*, 2626-2633.

[94] Green, N., Morgan, H. *Journal of Physics D-Applied Physics* 1997, *30*, L41-L44.

[95] Martinez-Duarte, R. *Electrophoresis* 2012, *33*, 3110-3132.

[96] Gascoyne, P., Vykoukal, J. *Electrophoresis* 2002, *23*, 1973-1983.

[97] Brown, A., Betts, W., Harrison, A., O'Neill, J. *Biosens. Bioelectron.* 1999, *14*, 341-351.

[98] Betts, W. *Trends Food Sci. Technol.* 1995, *6*, 51-58.

[99] Markx, G., Dyda, P., Pethig, R. *J. Biotechnol.* 1996, *51*, 175-180.

[100] Pethig, R., Markx, G. *Trends Biotechnol.* 1997, *15*, 426-432.

[101] Archer, G., Render, M., Betts, W., Sancho, M. *Microbios* 1993, *76*, 237-244.

[102] Cummings, E., Singh, A. *Microfluidic Devices and Systems Iii* 2000, *4177*, 164-173.

[103] Chou, C. F., Tegenfeldt, J. O., Bakajin, O., et al. *Biophysical Journal* 2002, *83*, 2170-2179.

[104] Zhou, G., Imamura, M., Suehiro, J., Hara, M. *Conference Record of the 2002 Ieee Industry Applications Conference, Vols 1-4* 2002, 1404-1411.

[105] Suehiro, J., Zhou, G., Imamura, M., Hara, M. *IEEE Trans. Ind. Appl.* 2003, *39*, 1514-1521.

[106] Kwon, J., Maeng, J., Chun, M., Song, S. *Microfluidics and Nanofluidics* 2008, *5*, 23-31.

[107] Lapizco-Encinas, B., Simmons, B., Cummings, E., Fintschenko, Y. *Electrophoresis* 2004, *25*, 1695-1704.

3 Electric Field Gradients in Micro/Nanofluidic Devices[1]

3.1 Introduction

Microfluidics has been a rapidly growing field during the last decade. Recent developments in microfabrication and micro-instrumentation have enabled the fabrication of microdevices that have high functionality and complexity and can carry out most chemical and biochemical processes. The miniaturization of these processes, which led to the creation of lab-on-a-chip systems, necessitates developing new methods of manipulating transport in micro scale environments. Since most liquid-solid interfaces bear an electrostatic charge, the application of an externally applied electric field results in the motion of the interface, a phenomenon called electrokinesis, which is one of the most frequently used methods to control the transport phenomena in microfluidics. Basic electrokinetic phenomena such as electroosmosis or electrophoresis, where the applied electric field acts as the driving force, were employed in a variety of applications such as gel electrophoresis [1, 2], chromatography [3, 4], capillary gel electrophoresis [5, 6], pulsed field electrophoresis [7], insulated-based dielectrophoresis [8], electrodeless dielectrophoresis [9]. The adaptation of these techniques on microfluidic platforms has opened the possibilities of having lab-on-a-chip devices. In order to design a successful electrokinetic process, it is important to have a precise knowledge of parameters affecting electrokinetic transport. One of these parameters is the applied electric field. The effects of the electric field and field gradients as important operational variables on electrophoresis and dielectrophoresis in microfabricated devices have been discussed in the literature [10-12]. For some processes, the nominal value of the field is sufficient to yield a correct calculation of the electrokinetic transport. However, when the local values

---

[1] A version of this chapter is published in Proceedings of ASME 2012 International Mechanical Engineering Congress and Exposition.

of the field deviate significantly from the nominal values, the assumption of a homogeneous field is an oversimplification resulting in either failed or low efficiency processes. For instance, during the electrophoresis separation of DNA, the presence of field inhomogeneities can significantly compromise the separation resolution by increasing the band broadening. Large gradients of the field can also affect the mobility or trajectory of molecules by introducing dielectrophoresis. This chapter studies the potential sources of inducing field gradients and their implications. By using finite element methods, the effects of the microchip geometry and the channels surface charge on the field magnitude and orientation have been evaluated. Of particular interest are microfabricated arrays used extensively in microfluidic devices either as sieving matrices or mixing enhancers. A comprehensive parametric study is conducted to determine how the posts arrangements, distance and size, and surface charge change the field gradients.

3.2 Method

3.2.1 Mathematical Model

Electrokinetic processes can be described by the governing laws of electric fields, flow, species transport, heat transfer and chemical reactions. Many comprehensive works on solving the flow and electric field equations for the flow in microdevices have been published. The studies by Probstein [13], Hunter [14] and Deen [15] provide more complete discussions of the electrokinetic equations. Several studies have investigated various microfluidic chips consisting of transverse microchannels [16-19] and porous structures [20-23] for different purposes of sample pretreatment and separation and detection of cells, particles and biomolecules. The geometry studied here (shown in Figure 3.1) is a common microfluidic chip design that has been used in other studies such as those involving analysis and fractionation of DNA molecules [24, 25]. As Figure 3.1 shows, the microchip consists of a square chamber with a packed array of micron scale posts, an injection channel, and several microchannels which surround the chamber and connect it to the electrodes, where the voltages are applied. The height of the posts is the same as chamber and microchannels.

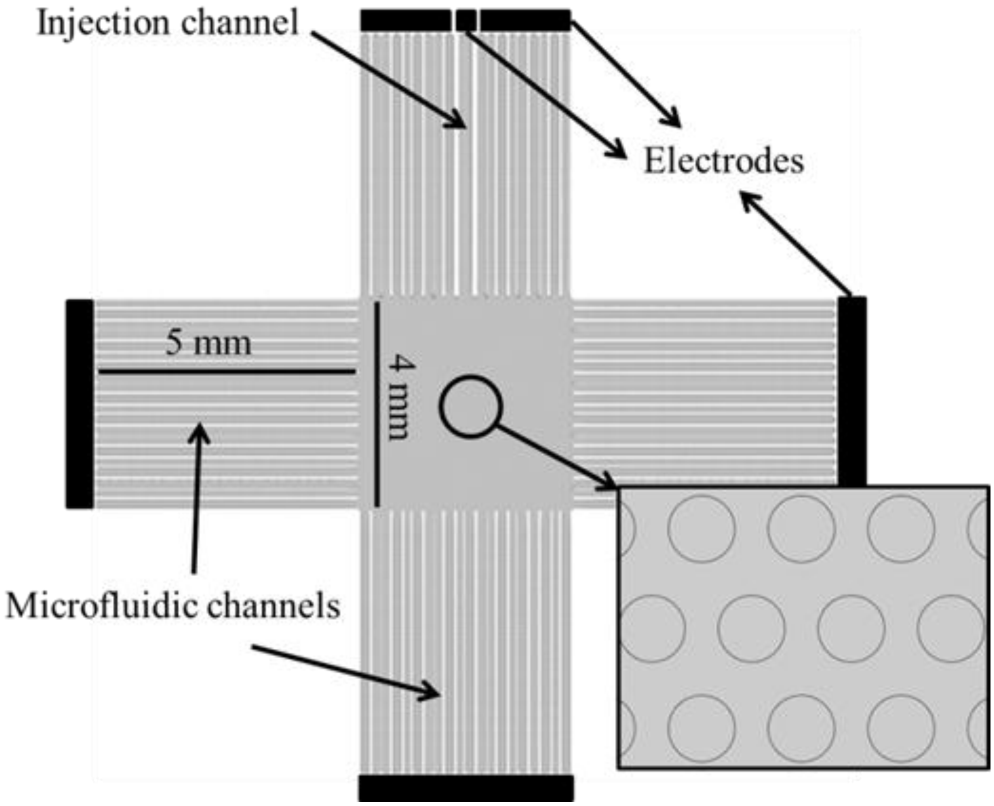

Figure 3.1 Schematic of the microfluidic chip studied in this work. The middle chamber consists of microfabricated arrays of posts. The injection channel and all the side microchannels are connected to the reservoirs where electrodes are used to apply electric voltages.

Our aim here is to calculate the electric field generated inside the microchip by applying the certain voltages at the channel reservoirs. We start our analysis with the conservation law for the chemical species in a fluid medium [26]

$$\frac{\partial c_i}{\partial t} = -\nabla . j_i + R_i \tag{3.1}$$

where c_i is the concentration of the i^{th} species, j_i is the i^{th} species flux, and R_i is the rate of production due to chemical reactions per unit volume. j_i has the contributions from convection, diffusion and migration under the influence of external forces. The external force here is the electrical force produced by applying voltages on the channels. Therefore, j_i can be obtained from the Nernst – Planck equation [26]

$$j_i = c_i\, u - D_i \nabla \mathrm{c} - \mu_i c_i \nabla \psi \qquad (3.2)$$

where D_i is the diffusivity of the i^{th} species, μ_i is mobility of the i^{th} species, and ψ is the electrical potential. In the steady state condition and the absence of chemical reaction, Eq. 3.1 will be reduced to

$$\nabla . j_i = 0 \qquad (3.3)$$

The current density, which is the result of the individual flux of all the ionic species present in the electrolyte solution, is given by [26]

$$i = \bar{F} \sum z_i\, j_i \qquad (3.4)$$

where $\bar{F}$ is the Faraday constant, and z_i is the valence of the i^{th} species. In terms of the ionic molar concentration, Eq. 3.2, Eq. 3.4 can be written as

$$\begin{aligned} i = \bar{F}u \sum z_i\; c_i - \bar{F} \sum D_i\, z_i \nabla c_i \\ - \frac{\bar{F}^2}{\bar{R}T} \nabla\psi \sum z_i^2\, D_i c_i \end{aligned} \qquad (3.5)$$

where $\bar{R}$ is the gas constant. In an electrically neutral electrolyte solution, $\sum z_i\, c_i = 0$, with no concentration gradient, $\nabla c_i = 0$, Eq. 3.5 is reduced to

$$i = -\sigma_m \nabla\psi \qquad (3.6)$$

where

$$\sigma_m = \frac{F^2}{RT}\left[\sum z_i^2 D_i c_i\right] \qquad (3.7)$$

and σ_m is the electric conductivity of the solution. Taking the divergence of the Eq. 3.4 gives

$$\nabla . i = F \sum z_i (\nabla . j_i) \qquad (3.8)$$

Considering Eq. 3.3, one can write

$$\nabla . i = 0 \qquad (3.9)$$

Substituting Eq. 3.6 into Eq. 3.9 yields the Laplace equation for the potential

$$\nabla^2 \psi = 0 \qquad (3.10)$$

Throughout the analysis above, the mobility, diffusivity and conductivity were assumed to be constant.

3.2.2 Numerical Simulation

The finite element method was used to calculate the electric field by solving Eq. 3.2 in the two dimensional geometry shown in Figure 3.1. The commercially available software COMSOL 3.5a was used to carry out the numerical simulation. By using COMSOL's Multiphysics capabilities, two series of simulations were performed in this study. The electrostatic mode was used, which solves the following equation

$$-\nabla \cdot \bar{d}\varepsilon_0\varepsilon_r\nabla\psi = \bar{d}\rho \qquad (3.11)$$

where $\bar{d}$ is the thickness of the device, ε_0 is the vacuum permittivity, ε_r is the relative permittivity, and ρ is the space charge density. The values of these parameters employed in our simulations are listed in Table 3.1.

Table 3.1 Values of physicochemical properties of the modeled system employed in the simulations

parameter	value	unit
thickness of the microdevice, $\bar{d}$	10	µm
space charge density, ρ	0	C/m^3
permittivity of free space, ε_0	8.85×10^{-12}	C/V.m
relative permittivity of the medium, ε_r	70	-
relative permittivity of the posts, ε_p	1.5	-

Since d, ε_0, ε_r, and ρ are constant values, the Eq. 8 is simplified to

$$-\nabla^2\psi = 0 \tag{3.12}$$

As was expected, the model solves the Laplace equation for the potential field. The electric field is obtained by solving the equation $E = -\nabla\psi$. Figure 3.2 illustrates the geometry of the 2D microfluidic chip studied in our simulations.

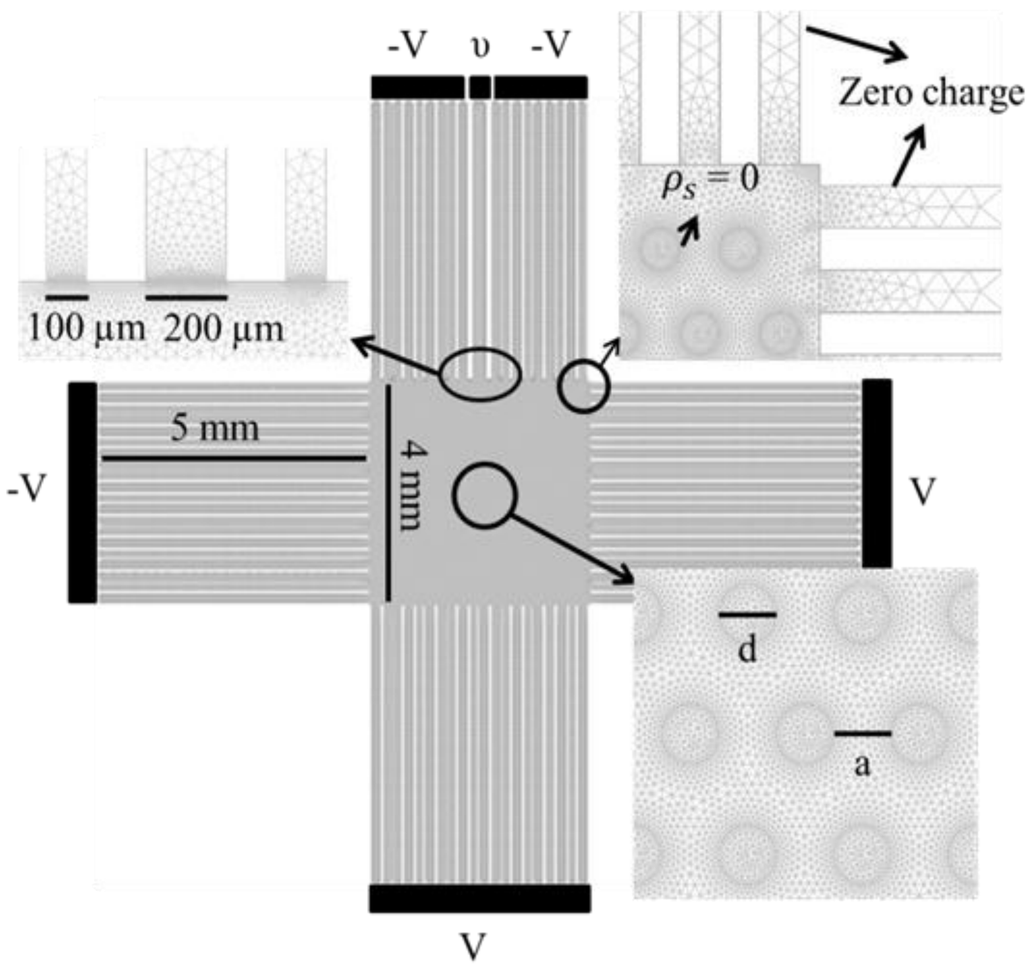

Figure 3.2 Schematic of the geometry solved in our simulations, illustrating the dimensions and boundary conditions. The middle chamber consisting of a post array is 4 mm × 4 mm, and the posts are of diameter d and surface-to-surface spacing a. The

channels, which are 5 mm in length, were connected to electrodes where certain voltages were applied. The surface charge of the posts (ρ_s) is zero and the zero charge condition is applied to the interior surface of the channels.

It consists of a 4 × 4 mm^2 square chamber connected to 20 microchannels (100 µm × 5 mm, 100 µm periodically) on three sides and 18 microchannels and an injection channel (200 µm × 5 mm) on the fourth side. The default boundary conditions are zero charge everywhere except on the reservoirs where specific voltages were applied. All the reservoirs on the top and left hand side of the chamber carry the same potential of -V, the reservoirs on the bottom and right-hand side of the chamber have the same potential of V, and the injection channel receives a smaller potential υ. Table 3.2 presents the ranges of V and υ employed in the simulations.

Table 3.2 The ranges of some parameters in the simulations

parameter	value	unit
magnitude of the voltages applied on the microchannels, V	(70 – 280)	V
voltage applied on the injection channel, υ	(-160 - -40)	V
diameter of the posts, d	(25 – 400)	µm
spacing between the posts, a	(25 – 400)	µm

Two series of simulations were conducted: i) the electric field orientation inside the microchip was calculated to define a domain inside the chamber where the field orientations are the same as the nominal values. In this part, the chamber did not contain the post arrays, ii) the electric field gradients were calculated in the chamber with a post array. The array consists of a regular lattice of posts of diameter *d* and surface-to-surface spacing *a*. The ranges of *d* and *a* employed in our simulations are presented in Table 3.2.

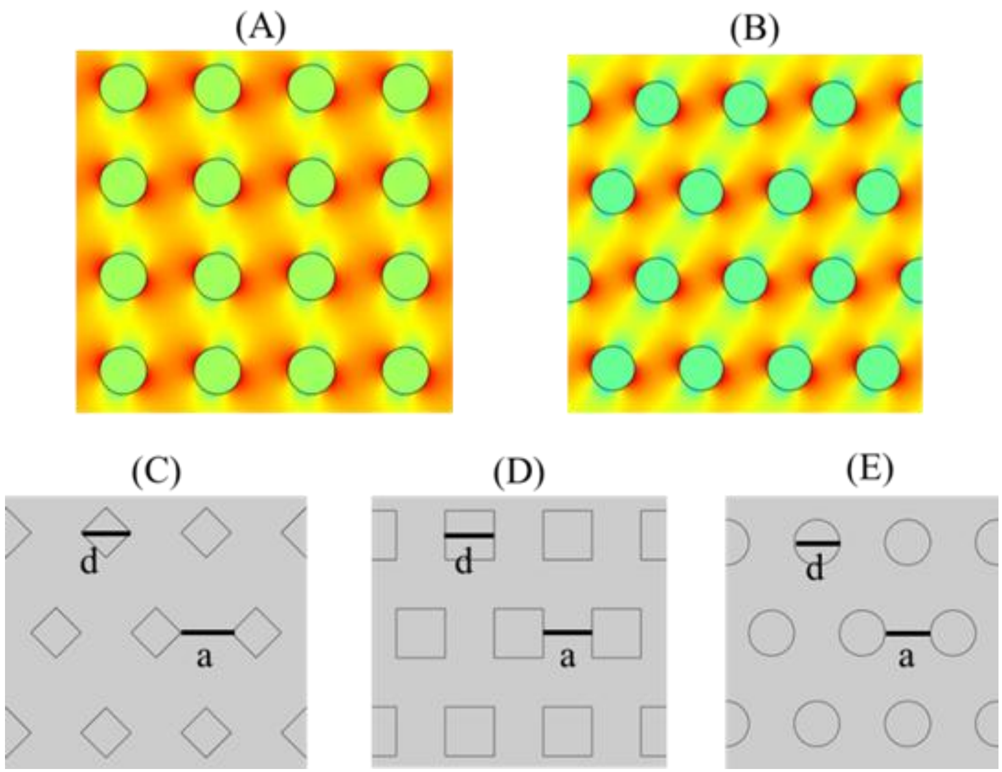

Figure 3.3 Schematic representation of (A) square and (B) hexagonal arrangements of microfabricated array with the posts of (C) rhombic type, (D) rectangular type and (E) circular type.

Hexagonal and square arrangements of the arrays (Figure 3.3 A and B), and circular, rectangular, and rhombic post cross-sections (Figure 3.3 C, D, and E) were considered. A triangular mesh configuration was used to discretize the geometry in order to solve the Laplace equation. Instead of a uniform mesh configuration, a more refined mesh configuration was used in the vicinity of the posts, sharp corners, and along the intersection to insure the accuracy of the calculation. Finite element analysis was applied in a triangular mesh of around 400 000 elements and 200 000 nodal points. It was observed that such a refined mesh configuration was sufficient to provide electric field values which were independent of the number of elements.

3.3 Results and Discussion

3.3.1 Electric Field Orientation

The 2D simulation with COMSOL Multiphysics provided a measure to define an area where the field orientation can be assumed to be constant and equal to its nominal value. In this study, this area will be called the “safe zone”. Figure 3.4 A depicts the safe zone for a symmetric microchip. The difference between this geometry and that show in Figure 3.2 is that the injection channel is replaced by two microchannels, so that all four sides of the chamber are exactly the same. It can be seen from the Figure 3.4 that the safe zone is a square in the middle of the microchip with equal spacing from the sides of the chamber. In order to investigate the effect of size, three microchips of different sizes (2mm, 4mm and 8mm chambers) were considered with the applied voltages being changed proportionally to the size to maintain the same field strengths. It was observed that the safe zone was linearly proportional in size to the microchip size and that the sufficient spacing from the sides of the chamber was 14.5% of the chamber size for a chamber of any size. Figure 3.4 B depicts the safe zone for the microchip shown in Figure 3.2 with the injection channel. The addition of the injection channel rendered the geometry asymmetric and consequently shrank the dimensions of the safe zone. The Figure 3.4 A and B show that the spacing between the safe zone and the chamber wall was changed from 14.5 % to 23 % by the addition of the injection channel.

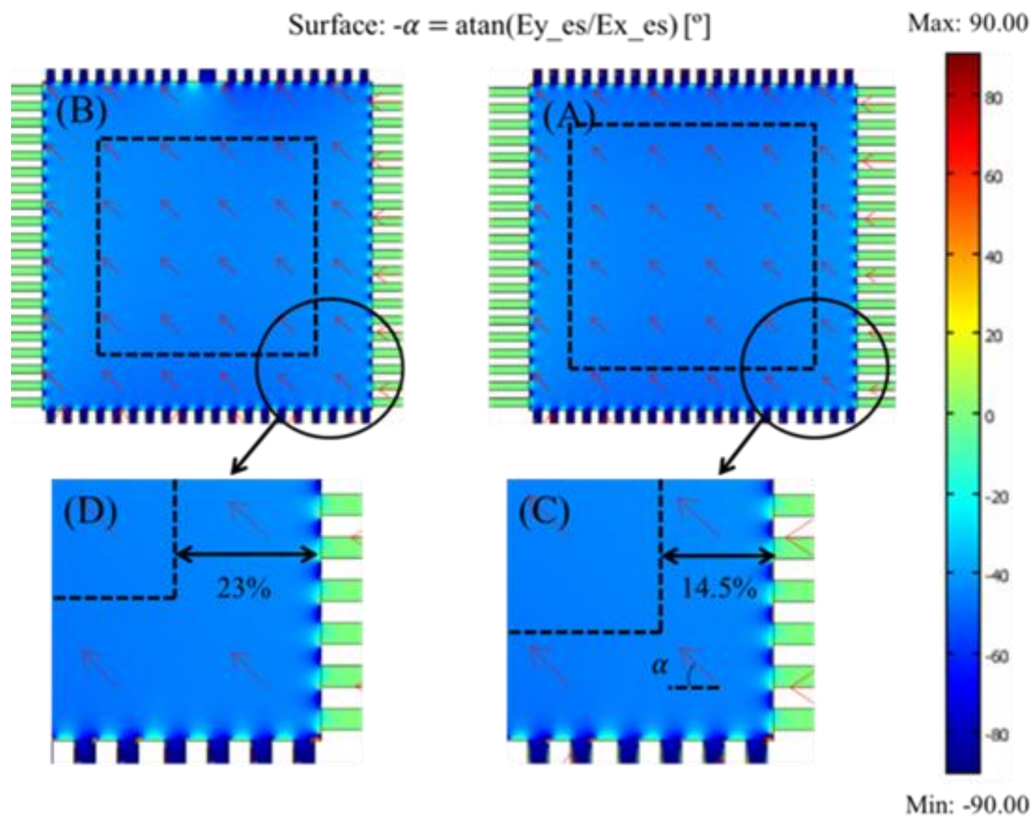

Figure 3.4 Schematic representation of the safe zone for (A) a symmetric geometry with no injection channel and (B) the asymmetric geometry shown in **Figure 3.2**. Spacing between the safe zone and the chamber walls is (C) 14.5% of the chamber size for the symmetric geometry and (D) 23% for the asymmetric geometry.

After changing the difference between the voltage applied at the injection channel (υ) and the voltage applied at the other channels (V), it was observed that the size of the safe zone was decreased by increasing the voltage difference (V-υ) as shown in Figure 3.5.

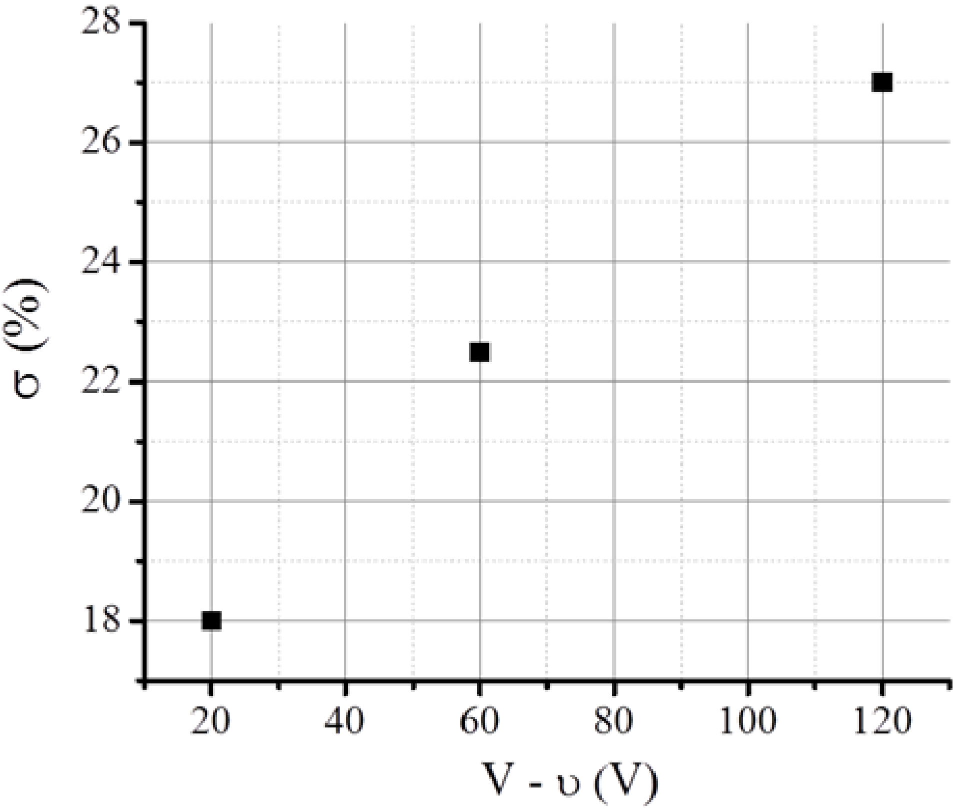

Figure 3.5 Spacing between the safe zone and the chamber walls, σ (shown as the percentage of the chamber size), versus voltage difference of the injection channel and microchannels ($V-\upsilon$).

The effect of the surface charge of the interior surfaces of the chamber and the channels on the shape and size of the safe zone was also studied, and the results are shown in Figure 3.6. Figure 3.6 A and B illustrate how the safe zone varied with different values of the surface charge. It can be seen that positive and negative charges had different influences on the safe zone.

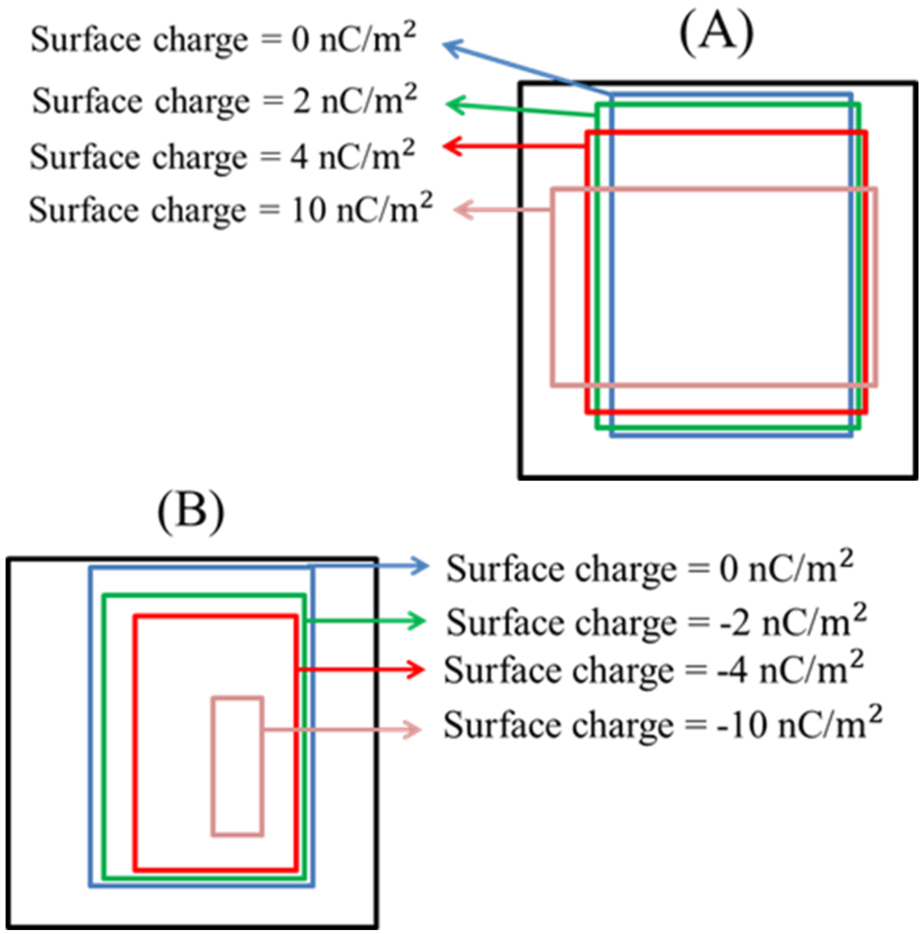

Figure 3.6 Schematic illustrating the effect of (A) positive surface charges and (B) negative surface charges on the shape and size of the safe zone.

3.3.2 Electric Field and Field Gradients

The electric field and field gradients were calculated in the microchip shown in Figure 3.2 where the chamber consists of arrays of posts. A parametric study was conducted to investigate the effect of diameter, distance between the posts, shape of the posts, and the post array arrangement on the electric field and field gradients. Figure 3.7 A shows the electric field calculated in a microfabricated array geometry with circular posts. In order to minimize the effects of the channel wall on the results, a unit cell in the middle of the chamber was considered where the field and field gradients were averaged over area of the unit cell as shown in

Figure 3.7 B. In what follows, the values of the field and field gradients employed to make the graphs are the averaged values over this area. Figure 3.8 presents the variation of the field with respect to the distance between the posts, *a*, for three post cross sections: circular, rectangular, and rhombic. The value of the diameter was kept constant and equal to 100μm. It is evident from Figure 3.8 that the electric field decreased as the distance increased, regardless of the post shape. For each value of *a*, the greatest value of the field belongs to the rectangular posts, and the lowest value belongs to the rhombic posts.

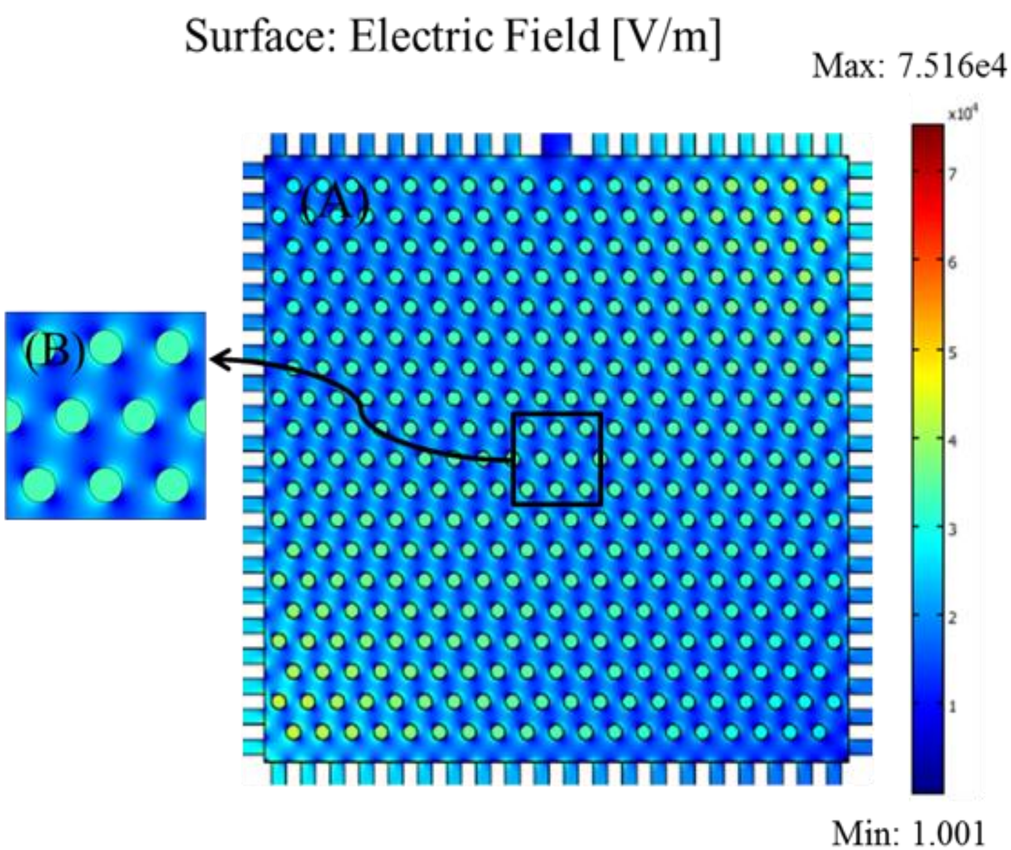

Figure 3.7 (A) Electric field calculated in a microfabricated array arrangement with circular posts. (B) Schematic presentation of the unit cell over which the averages of the field and field gradients employed in our evaluations in this work, were calculated.

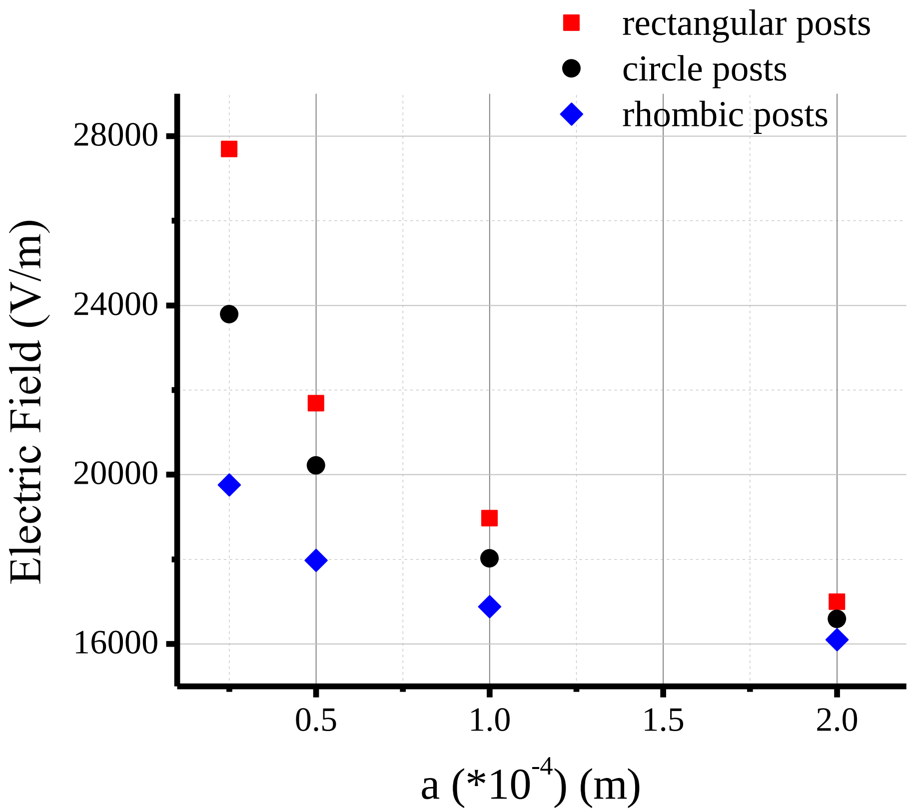

Figure 3.8 Variation of the electric field with respect to distance between the posts for the posts of different types: circular, rectangular and rhombic. The field decreases as the distance increases.

The variation of the field with respect to the diameter of the posts was evaluated as well.

Figure 3.9 plots the electric field versus the diameter of the posts for all circular, rectangular and rhombic posts. Note that the post-to-post distance was kept constant and equal to 100µm.

Figure 3.9 reveals that the field is increased by increasing the diameter of the posts. This figure also shows that the effect of the diameter on the value of the electric field for the rectangular posts is more than that for the circular and rhombic posts; i.e., when the diameter of the post is changed, the structure which has rectangular posts experiences the most variation in the value of the electric field compared to the structures with circular or rhombic posts.

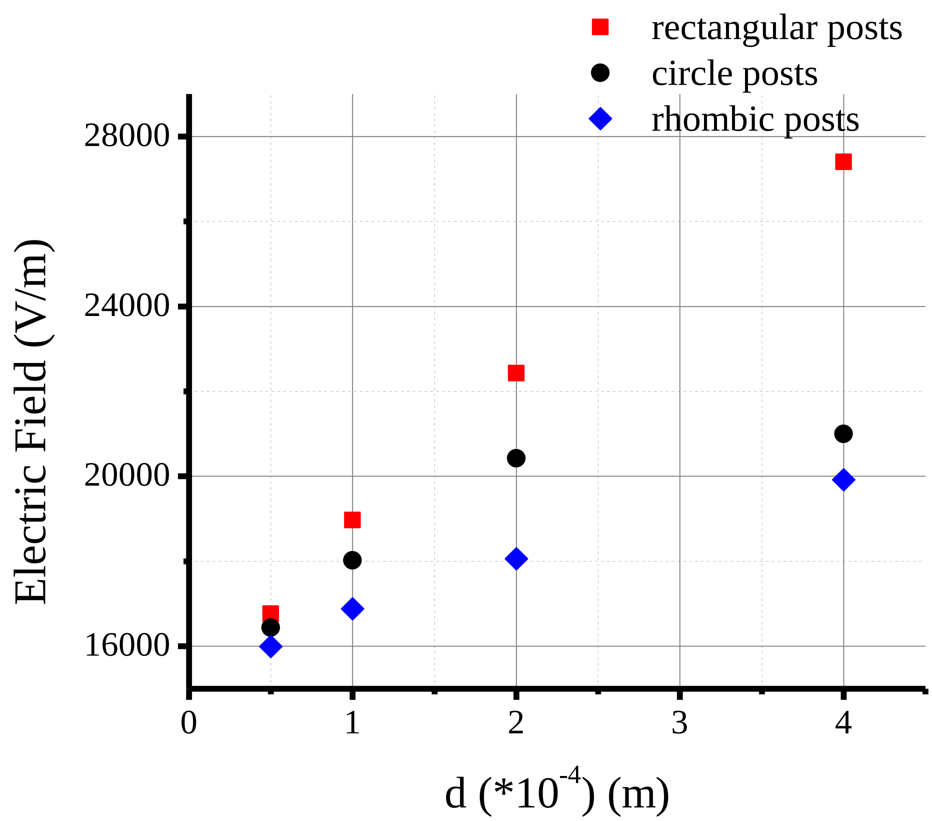

Figure 3.9 Relation between the field and diameter of the posts for circular, rectangular and rhombic posts. Increasing the diameter of the posts increases the field.

Figure 3.10 presents the distribution of the electric field over the unit cell area for three types of posts (circular, rectangular and rhombic). This figure shows that the extremums of the electric field take place in the corners of the posts for rectangular posts (Figure 3.10 B). For circular posts, the extremums take place in the direction of the electric field orientation (Figure 3.10 A).

In the structure with rhombic posts, the field extremums are located in the corners of the posts and also in the direction of the field orientation (Figure 3.10 C). As one can see from Figure 3.10 B, the field orientation is in the direction of the diagonal of the rectangular posts and also for a specific structure with the same values of *d* and *a*, the geometry with rectangular posts experiences the highest maximum value of the electric field rather than the structures with circular or rhombic posts. Regarding the variation of the field with respect to the diameter and distance between the posts (Figure 3.8 and Figure 3.9), we also evaluated the relation between the field and *d/a* ratio.

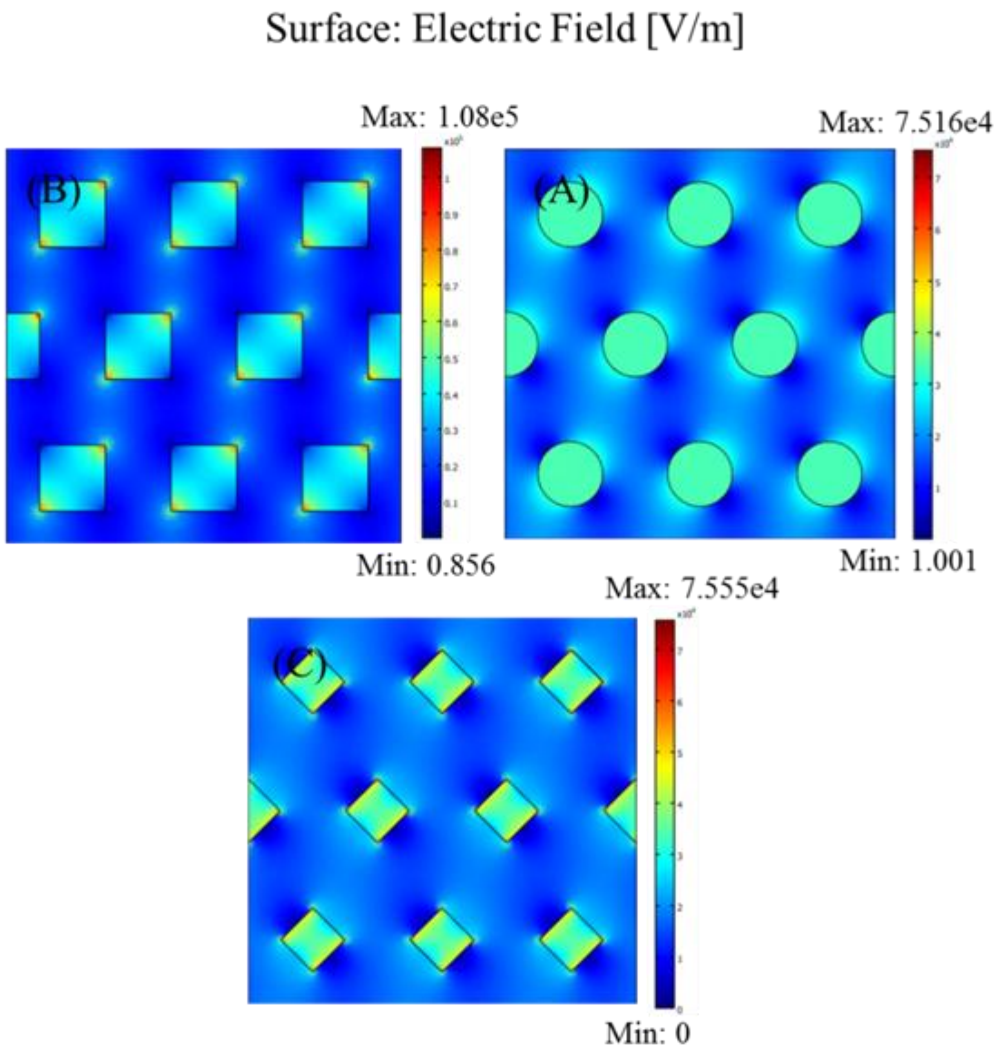

Figure 3.10 Schematic illustrates the electric field distribution and position of the field local extremums in the structures with (A) circular posts (B) rectangular posts and (C) rhombic posts.

Figure 3.11 plots the field versus *d/a* ratio. It can be observed from this figure that increasing the *d/a* ratio increases the field monotonously.

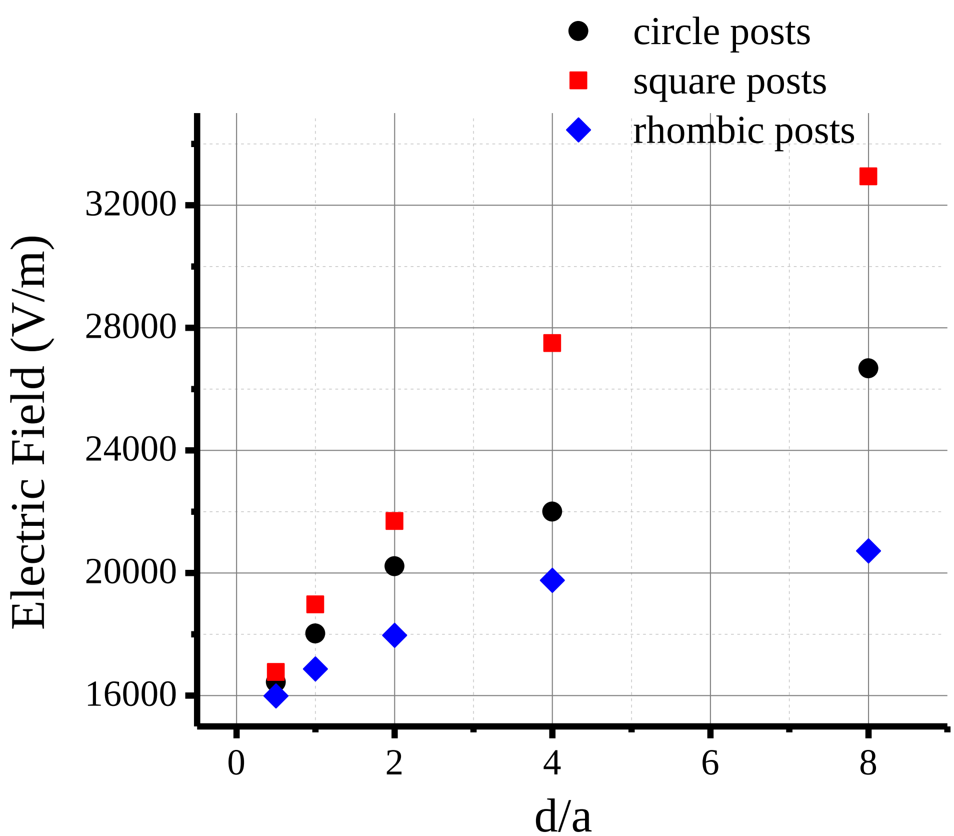

Figure 3.11 Relation between the field and *d/a* ratio for circular, rectangular and rhombic posts. The field monotonously increases as *d/a* ratio increases.

Since the *d/a* ratio is a combination of the diameter and distance between the posts, it can be used as a meaningful parameter in designing the microstructures including the post arrays. Figure 3.12 plots the field gradients versus the distance between the posts, *a*. According to Figure 3.12, the field gradient decreases as the distance between the posts increases. Also, this figure demonstrates that for all values of *a*, the highest field gradient is present for the geometry with rectangular posts.

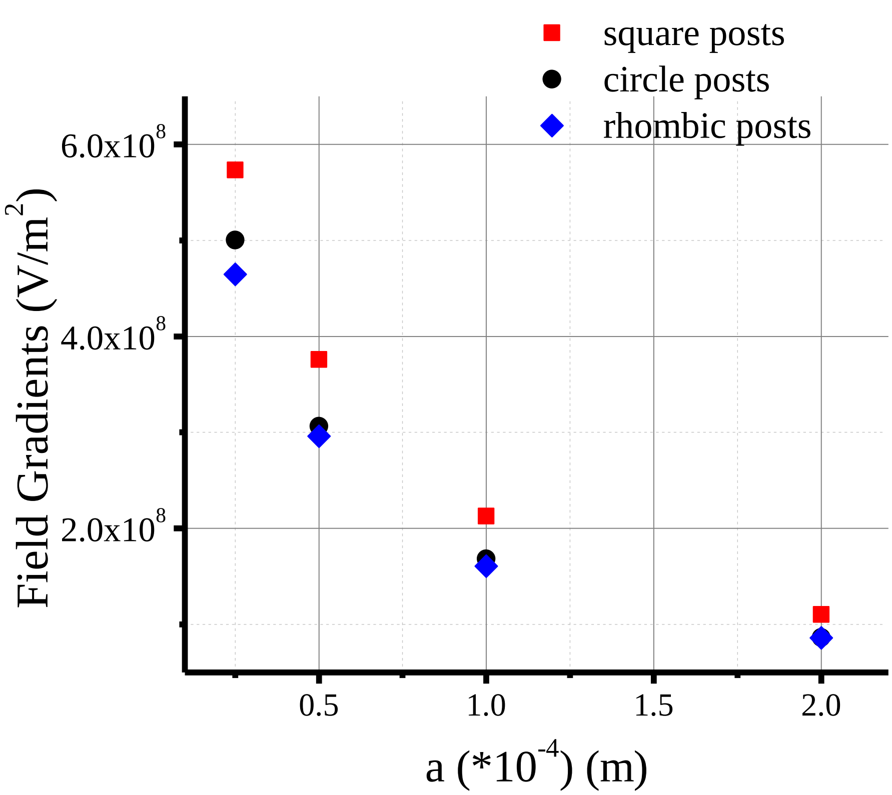

Figure 3.12 Variation of the field gradients with respect to distance between the posts for the posts of different type: circular, rectangular and rhombic. The field gradients decrease as the distance increases.

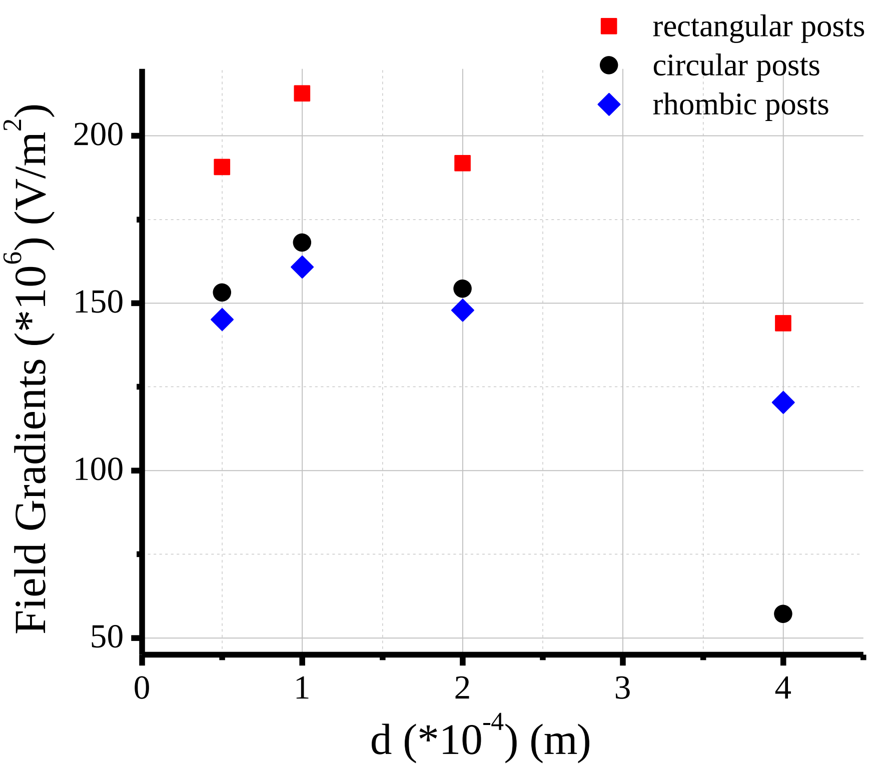

Figure 3.13 Relation between the field gradients and diameter of the posts. The variation of the field gradients with respect to diameter is not monotonous. The geometry with rectangular posts experiences the highest field gradients compared to the geometries with circular or rhombic posts.

Figure 3.13 shows the variation of the field gradients with respect to the diameter of the posts. It can be seen from this figure that changing the diameter of the posts does not change the field gradients monotonously and also that for all values of d, the highest field gradients belong to the structure with rectangular posts.

Seeking a parameter with which the field gradient varies monotonously, we came up with the parameter $N.d.a^{-1}$. N is total number of the posts in each structure. Figure 3.14 plots the variation of the field gradients with respect to $N.d.a^{-1}$. Formerly it was found that increasing the d/a ratio increased the field monotonously. Figure 3.14 demonstrates that the field gradients were monotonously increased by increasing $N.d.a^{-1}$, which is the product of the total number of the posts and the *d/a* ratio. Therefore, this parameter can be employed in designing the microstructures with post arrays for the applications in which the field gradient is important.

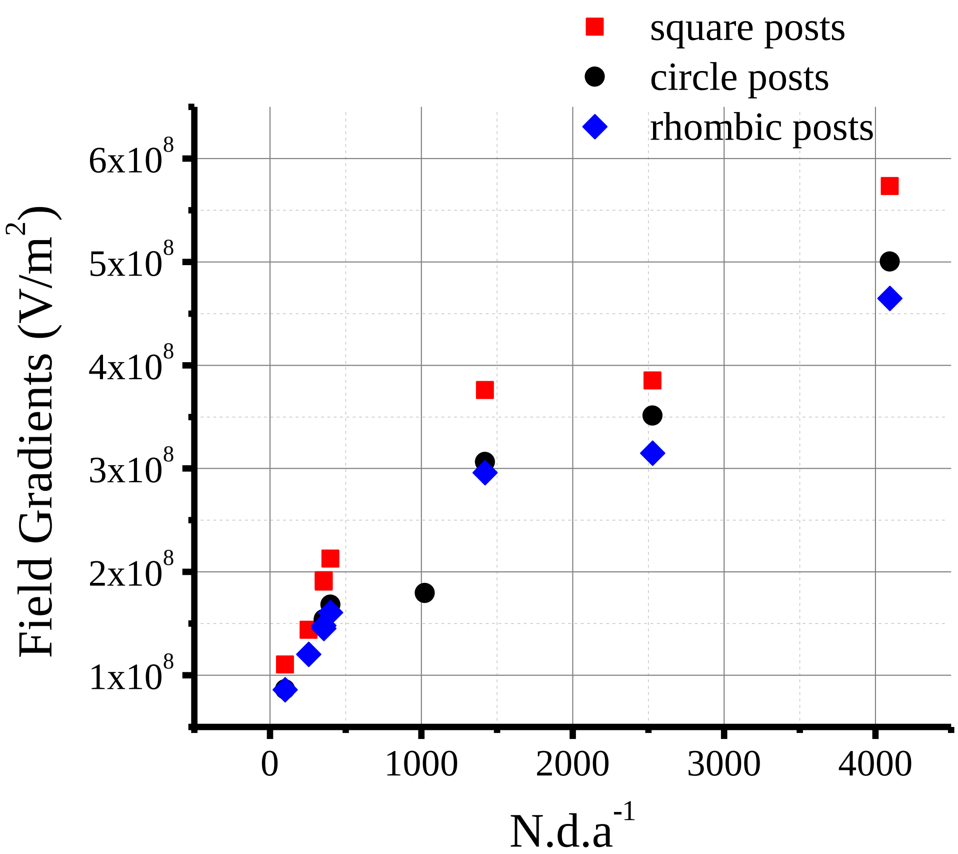

Figure 3.14 Variation of the field gradients with respect to the parameter $N.d.a^{-1}$ for circular, rectangular and rhombic posts.

Figure 3.15 illustrates the distribution of the field gradients over the unit cell area for the structures with circular, rectangular and rhombic posts. The extremums of the field gradients take place in the corners of the rectangular and rhombic posts. It can be observed from this figure that the highest field gradients belong to the geometry with rectangular posts and then to the geometry with rhombic posts.

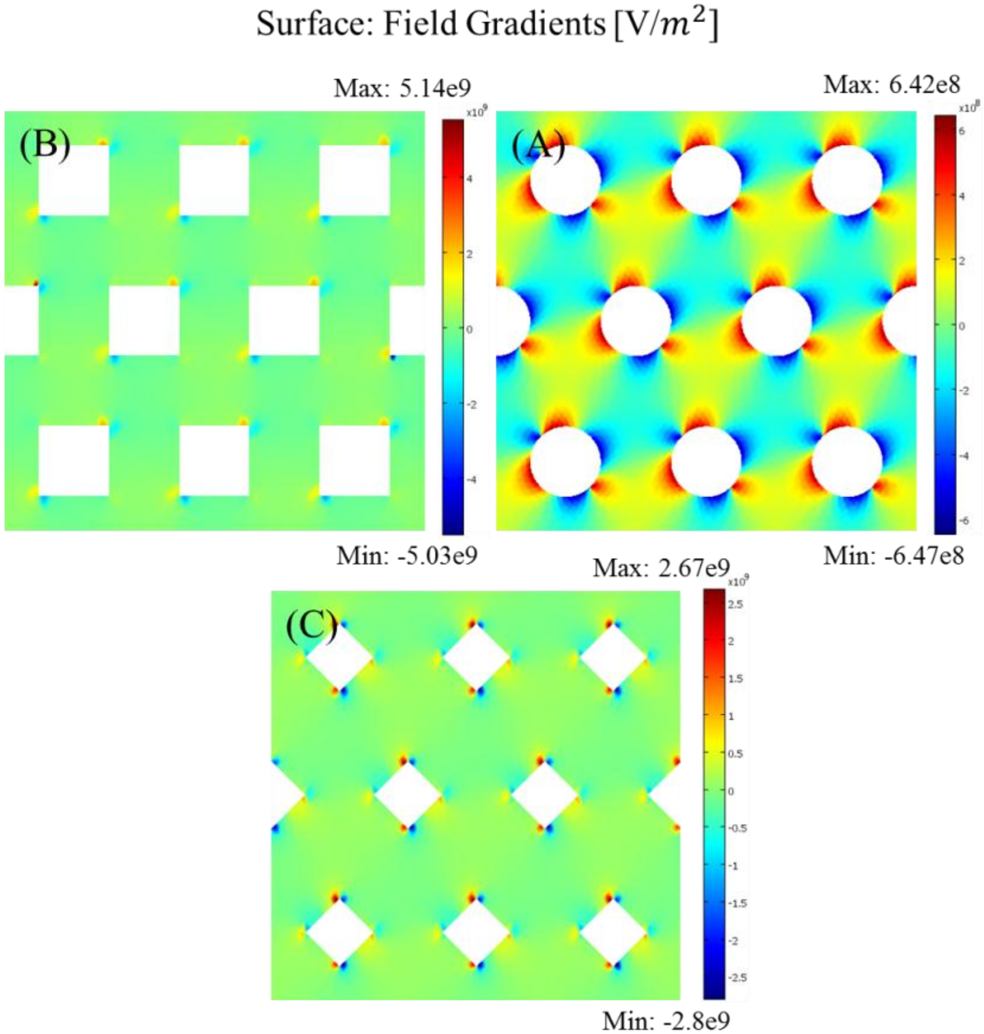

Figure 3.15 Schematic representation of the field gradients and their extremums over the unit cells of structures with (A) circular posts, (B) rectangular posts and (C) rhombic posts. The highest field gradient belongs to the structure with rectangular posts.

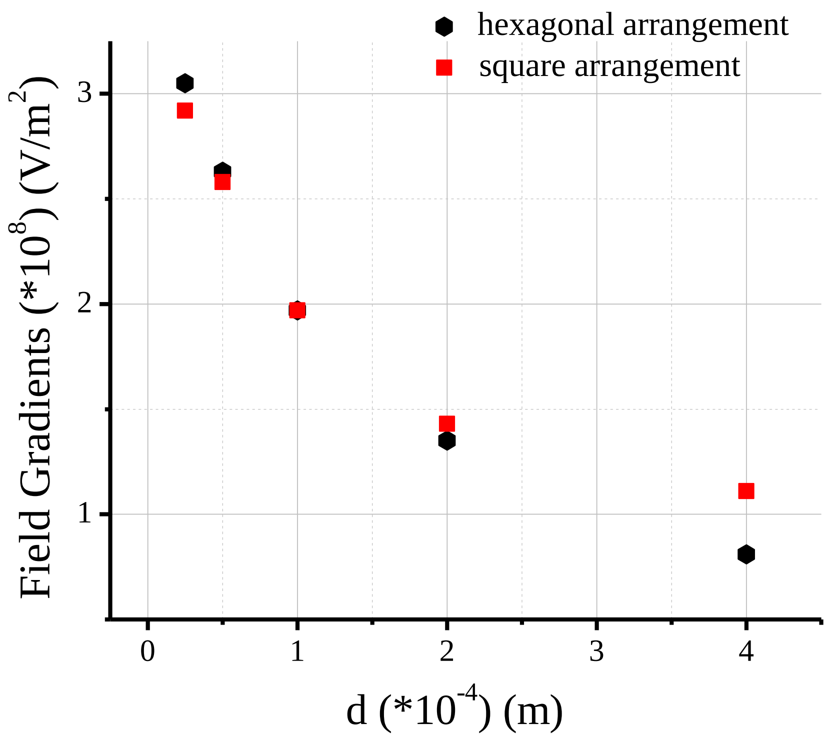

Figure 3.16 Variation of the field gradient with respect to diameter for the circular posts in two different arrangements: hexagonal and square.

To investigate the effect of post arrangement on the field gradients, structures with a square arrangement were created, and the results are presented in Figure 3.16. This figure shows that for $d<a$, the square arrangement provided larger values of the field gradients than those provided by the hexagonal arrangement. On the other hand, for $d>a$, the hexagonal arrangement yielded larger field gradients. For $d = a$, both arrangements experienced equal values of the field gradients.

3.4 Conclusion

The electric field gradient and orientation in a microfabricated array structure was calculated numerically by using the finite element method. It was observed that in the vicinity of the junction between the chamber and microchannels, the field orientation significantly deviated from its nominal values. We defined a “safe zone” in the chamber where this deviation was less than 5%. Our calculations showed that the dimension of this zone was affected by the chamber size, channels surface charge, and the difference between the voltages applied at the injection channel and side channels. A symmetric microchip with zero surface charge on the wall had the largest safe zone meaning it can maintain the nominal values of the field orientation across the chamber.

The electric field and field gradient were also calculated in a microfabricated array geometry. It was observed that increasing the diameter and decreasing the post-to-post distance increased the electric field. It was also found that increasing the *d/a* ratio increased the field monotonously. Thus, this parameter can help in designing the microfabricated structures with the arrays of posts which have applications where the electric field value is important. In addition, it was seen that the rectangular posts experienced the highest value of the electric field compared to those of the circular and rhombic posts.

The field gradients were observed to be decreased by an increase in post-to-post distance, but no relation was found between the field gradients and the diameter of the posts. It was obtained that parameter $N.d.a^{-1}$ increased the field gradients monotonously. This relation implies that in addition to *d* and *a*, the total number of the posts also affected the field gradients. $N.d.a^{-1}$ can be used in designing microfabricated devices with post arrays for applications in which the field gradients values are important. It was observed that the geometries with rectangular posts induced the highest values of the field gradients compared to those of the geometries with circular or rhombic posts. It was also observed that the extremums of the field gradients took place in the corners of the posts.

The effect of array arrangement on the field gradient was observed to depend on the d/a ratio. For $d/a < 1$, the square arrangement provided larger values of the field gradients, whereas, for $d/a > 1$, the hexagonal arrangement yielded larger field gradients. For $d/a = 1$, both arrangements exhibited the equal values of the field gradients.

References

[1] Guttman, A., Cooke, N. *Anal. Chem.* 1991, *63*, 2038-2042.

[2] Fang, Y., Zhang, J., Hou, J., Lu, H., Dovichi, N. *Electrophoresis* 1996, *17*, 1436-1442.

[3] De Pra, M., Kok, W. T., Schoenmakers, P. J. *Journal of Chromatography a* 2008, *1184*, 560-572.

[4] Moore, A. W., Jacobson, S. C., Ramsey, J. M. *Anal. Chem.* 1995, *67*, 4184-4189.

[5] Effenhaunser, C. S., Paulus, A., Manz, A., Widmer, H. M. *Anal. Chem.* 1994, *66*, 2949-2953.

[6] WOOLLEY, A., MATHIES, R. *Proc. Natl. Acad. Sci. U. S. A.* 1994, *91*, 11348-11352.

[7] Duke, T., Austin, R., Cox, E., Chan, S. *Electrophoresis* 1996, *17*, 1075-1079.

[8] Bhattacharya, S., Chao, T., Ros, A. *Electrophoresis* 2011, *32*, 2550-2558.

[9] Chou, C., Tegenfeldt, J., Bakajin, O., Chan, S. *et al*. *Biophys. J.* 2002, *83*, 2170-2179.

[10] Dorfman, K. D. *Reviews of Modern Physics* 2010, *82*, 2903-2947.

[11] Chen, G. D., Fachin, F., Fernandez-Suarez, M., Wardle, B. L., Toner, M. *Small* 2011, *7*, 1061-1067.

[12] Oh, D., Cheong, I. C., Lee, H. G., Eo, S. K., Kang, S. H. *Bulletin of the Korean Chemical Society* 2010, *31*, 1902-1906.

[13] Probstein, R. F. *Physicochemical hydrodynamics* , Wiley 1994.

[14] Hunter, R. J. *Foundations of colloid science*, Oxford, Oxford University Press 2001.

[15] Deen, W. M. *Analysis of transport phenomena*, Oxford, Oxford University Press 1998.

[16] Kang, C. M., Joo, S., Bae, J. H., Kirn, Y. *et al*. *Anal. Chem.* 2012, *84*, 901-907.

[17] Cheng, S., Wang, Z., Ge, S., Wang, H. *et al*. *Microchimica Acta* 2012, *176*, 295-301.

[18] Khandurina, J., Jacobson, S., Waters, L., Foote, R., Ramsey, J. *Anal. Chem.* 1999, *71*, 1815-1819.

[19] Kuo, C., Shiu, J., Wei, K. H., Chen, P. *Journal of Chromatography a* 2007, *1162*, 175-179.

[20] Shiu, J., Whang, W., Chen, P. *Journal of Chromatography a* 2008, *1206*, 72-76.

[21] Kang, Q., Li, Y., Xu, J., Su, L. *et al*. *Electrophoresis* 2010, *31*, 3028-3034.

[22] Xu, Y., Vaidya, B., Patel, A., Ford, S. *et al*. *Anal. Chem.* 2003, *75*, 2975-2984.

[23] Hanke, C., Waide, S., Kettler, R., Dittrich, P. S. *Analytical and Bioanalytical Chemistry* 2012, *402*, 2577-2585.

[24] Zeng, Y., He, M., Harrison, D. J. *Angewandte Chemie-International Edition* 2008, *47*, 6388-6391.

[25] Huang, L., Tegenfeldt, J., Kraeft, J., Sturm, J. *et al*. *Nat. Biotechnol.* 2002, *20*, 1048-1051.

[26] Masliyah, J. H., Bhattacharjee, S. *Electrokinetic and colloid transport phenomena*, Wiley 2006.

4 Electrophoresis and Dielectrophoresis in Microfabricated Post Arrays[2]

4.1 Introduction

During the last decade, there has been a significant development of microfluidic devices because of the increased interest in processes and devices that allow manipulation and assembly of structures from micro and nanosize particles [1]. One class of microfluidic devices are microfabricated post arrays (MFPA). The ability of MFPA to separate, manipulate, concentrate and sort particles according to size and shape is very useful in numerous fields including environmental, clinical and biological applications [2-7]. In this study, the particle transport in the presence of diffusion, electrophoresis (EP) and dielectrophoresis (DEP) effects in a MFPA is evaluated. Several criteria were defined based on physical and dielectric properties of the particle and medium, where one of the mentioned effects, i.e., diffusion, electrophoresis, or dielectrophoresis is the governing mechanism in particle transport. To this end, the fate of particles in terms of concentration profile is studied for various relative magnitudes of DEP and EP forces by varying the particle and medium properties.

Particle subjected to a spatially nonuniform electric field experiences electrical forces that can cause both electrophoresis and dielectrophoresis (DEP) [8-13]. Electrophoretic forces are well chronicled and generally result from the hydrodynamic frictional forces balancing electrostatic forces. For the DEP, the translational force can cause motion toward increasing local field strength (positive DEP) or decreasing field strength (negative DEP) [14]. The majority of the research studies on DEP have used alternating current (AC) electric fields and arrays of microelectrodes to create nonuniform electric fields resulting in high

---

[2] A version of this chapter has been submitted for publication to Electrophoresis journal.

electric field gradients through applying low voltages [15]. However, there are some disadvantages with this approach: high cost and complex fabrication processes for electrodes, and decrease of functionality due to fouling effects, which is a common effect when handling biological samples [16-18]. The alternative technique of carrying out DEP is DC DEP where the voltage is applied employing only two electrodes that straddle a post array structure. When an electric field is applied across an array of posts, the presence of the post structures creates regions of higher and lower field strength, resulting in the nonuniform electric field necessary for DEP to occur.

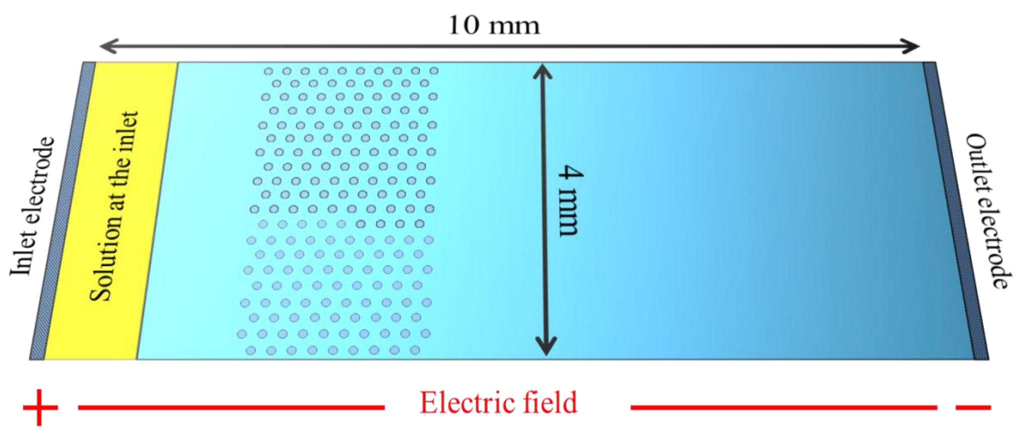

Figure 4.1 A Schematic representation of the 2D microchannel studied in this work. It consists of a microchannel 10 mm long, 4 mm wide and 10 μm deep, containing an array of 10 columns×20 rows of posts 100 μm in diameter and arranged 200 μm center to center. A suspending solution is introduced into the channel and a DC voltage is applied to electrodes located in remote inlet and outlet reservoirs.

In this manuscript, we evaluated the relative magnitude of DC dielectrophoresis and electrophoresis and its influence on concentration of particles through uniformly patterned arrays of posts. Employing DC electric field enables finer manipulation of particles, since the relative magnitude of electrophoresis and dielectrophoresis can be measured and manipulated. For example, in order to trap particles dielectrophoresis has to overcome both diffusion and electrophoresis.

This work presents the characterization of electrophoretic flow coupled with DC dielectrophoresis, to identify the operating conditions under which DEP particle trapping occurs and cannot be ignored. We show that microfabricated devices can be used to manipulate particles through the parameters affecting the response of the particles to the applied field, such as zeta potential of the particles, medium permittivity and particle size, by varying the relative magnitude of electrophoretic flow with respect to DEP. The geometry studied in this work (shown in Figure 4.1) is a typical design of microfluidic channel including arrays of micron-scale posts that has been used in several studies for different purposes such as dielectrophoretic concentration, passive mixing of nanoparticles, purification of DNA fragments, and bio-separation [7, 19-28] . A suspending solution is introduced into the channel and a DC voltage is applied to electrodes located in inlet and outlet reservoirs. Upon applying the electric field, the field nonuniformities are generated due to the presence of post arrays inside the microchannel. Electrophoresis is used to transport the particles through the channel. As the particles are migrating through the post array, they are concentrated according to their characteristic physical and dielectric properties in response to electrophoretic, dielectrophoretic, and Brownian forces. Particle concentration profiles were calculated by solving the convection-diffusion-migration equation of particles under EP, DEP, and Brownian forces using a finite element scheme. The objective was to define non-dimensional parameters based on the physical properties of particles and the medium to characterize the governing mechanism of particle transport through post arrays in the presence of field heterogeneities.

It is worth mentioning here that throughout this study, we assumed the fluid flow in the microchannel is very small compared to particle velocity and can be neglected. This assumption is originated from the observation that in the majority of the experimental applications involving post arrays, the surface of the posts and the microchannel walls were modified to bear zero surface charges in order to negate the electroosmosis velocity of the medium which has negative effects on the separation or mixing efficiency.

4.2 Theoretical

The transport of particles in a microchannel filled with conductive media through an array of micron scale posts is governed by the general mass conservation equation which has the following form

$$\frac{\partial c}{\partial t} = -\nabla . j + R \qquad (4.1)$$

Where *c* is the particle concentration, *j* is the particle flux and *R* is the rate of production due to chemical reaction per unit volume. *j* has the contributions from convection, diffusion, and migration under the influence of external forces [29]

$$j = c\,u - D.\nabla c + \frac{c\,D}{k_b\,T}\,F \qquad (4.2)$$

here, *u* is the fluid velocity, *D* is the particle diffusion coefficient, k_b is the Boltzmann constant, *T* is the absolute temperature, and *F* is the total force exerted on the particles. In the absence of any chemical reaction (*R*=0) in the stationary fluid flow (*u*=0), substituting *j* in Eq. 4.1 by its definition from Eq. 4.2, the convection-diffusion-migration equation (CDM) of the particles can be written as

$$\frac{\partial c}{\partial t} + \nabla.\left(c\,\frac{D}{k_b T}\,F - D\nabla c\right) = 0 \qquad (4.3)$$

The diffusion coefficient can be obtained from the following equation

$$D = \frac{k_b T}{6\pi\mu r} \qquad (4.4)$$

Where μ is the viscosity of the electrolyte solution and *r* is the particle radius. A suspended particle subjected to a spatially nonuniform electric field experiences electrical forces that can cause both electrophoresis and dielectrophoresis (DEP) [8-12, 19] . The total electrical force (*F*) exerted on a particle can be calculated by the sum of the electrophoretic and dielectrophoretic forces it experiences

$$F = F_{EP} + F_{DEP} \qquad (4.5)$$

For a spherical particle of radius r, in a high concentrated electrolyte solution, when the Debye screening layer is small relative to the particle radius, i.e., $\kappa r >> 1$, the electrophoretic force can be obtained from the following equation [29]

$$F_{EP} = 6\pi r \varepsilon_r \varepsilon_0 \zeta \, E \, (1 + \kappa r) \qquad (4.6)$$

Where ε_r is the relative permittivity of the medium, ε_0 is the permittivity of free space, ζ is the zeta potential at the particle surface and E is the externally applied electric field. Dielectrophoretic force exerted on a spherical particle in a nonuniform electric field is given by [14]

$$F_{DEP} = \pi \varepsilon_r \, \varepsilon_0 r^3 \, Re[f_{CM}] \, \nabla(E.E) \qquad (4.7)$$

Where $Re[f_{CM}]$ is the real part of the Clausius-Mossotti factor. In the low frequency or DC limit, the Clausius-Mossotti factor (consequently polarization) depends solely on the conductivity of the particle and suspending medium and can be approximated by [14]

$$f_{CM} = \frac{\sigma_p - \sigma_m}{\sigma_p + 2\sigma_m} \qquad (4.8)$$

Where σ_p and σ_m are the real conductivities of the particle and medium, respectively. Positive DEP (movement toward strong field region) occurs when a particle is more polarizable than the medium ($\sigma_p > \sigma_m$), whereas negative DEP (movement away from strong field region) happens if a particle is less polarizable ($\sigma_p < \sigma_m$). The particles considered in this study have higher conductivities than the medium and experience positive DEP.

4.3 Numerical Simulation

Finite element method was used to solve the convection-diffusion-migration equation (CDM) of the particles (Eq. 4.3) in the two dimensional geometry as shown in Figure 4.1. The numerical simulation is conducted using commercially available software, COMSOL Multiphysics.

The local values of electric field, *E*, in our geometry was calculated by solving the Laplace equation ($\nabla^2\psi = 0$) with the following boundary conditions:

$$n.I = 0 \quad \text{at the microchannel boundaries and around the posts} \tag{4.9}$$

$$\psi = \psi_{in} \quad \text{at channel inlet} \tag{4.10}$$

$$\psi = \psi_{out} \quad \text{at channel outlet} \tag{4.11}$$

where ψ is the electrical potential, *n* is the normal vector to the surface, *I* is the electrical current, and $\psi_{in} - \psi_{out}$ is the electrical potential applied between the electrodes. From the solution of Laplace equation, numerical values for the electric field and electric field gradients were obtained in the post array geometry. Using the local values of electric field and field gradients, the electrophoretic and dielectrophoretic forces can be calculated using Eqs. 4.6 and 4.7, respectively.

Figure 4.2 illustrates the geometry of the 2D microchannel studied in our simulations. It consists of a microchannel 10 mm long, 4 mm wide, and 10 μm deep, containing an array of 10 columns×20 rows of posts 100 μm in diameter and arranged 200 μm center to center. Hexagonal arrangement and circular cross-sectional posts were considered for the post array. A sample of 1mM of particle solution was introduced at the inlet reservoir, and electrodes placed at the reservoirs applied electric potential of 40 V across the microchannel.

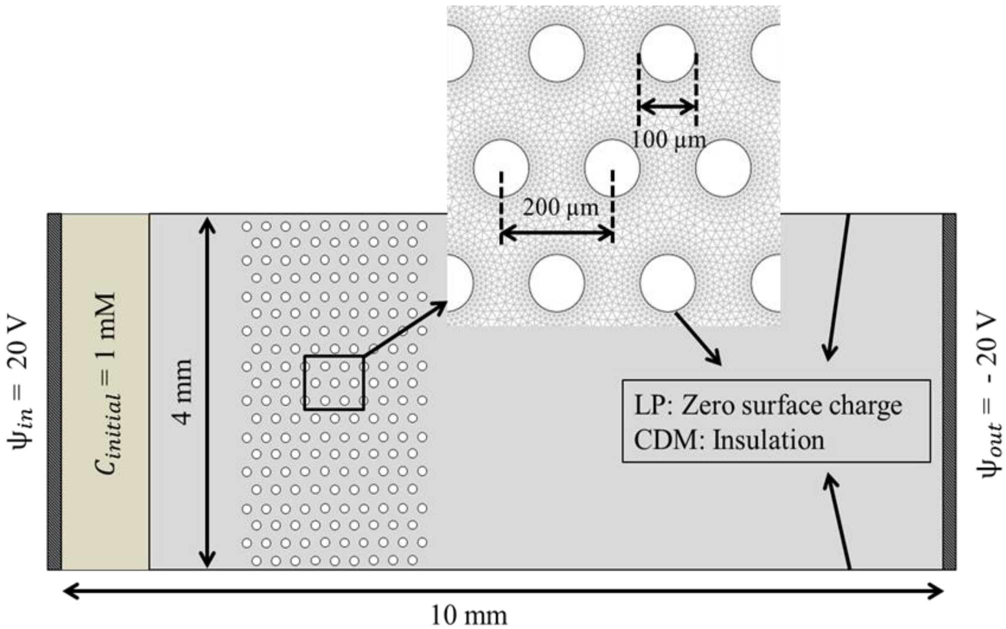

Figure 4.2 Schematic of the geometry solved in our simulations illustrating the dimensions, initial condition, and boundary conditions. It consists of a microchannel 10 mm long, 4 mm wide and 10 μm deep, containing an array of 10 columns×20 rows of posts 100 μm in diameter and arranged 200 μm center to center. Zero surface charge condition (for the Laplace equation) and insulation condition (for the CDM equation) are applied to the posts and the interior surface of the microchannel. A sample of 1mM of particle solution was introduced at the inlet reservoir, and electrodes placed at the reservoirs applied electric potential of 40 V across the microchannel.

The initial and boundary conditions employed in the simulations in order to solve the Laplace (LA) and convection-diffusion-migration (CDM) equation are presented in Figure 4.2. A triangular mesh configuration was used to discretize the geometry in order to solve both Laplace and convection diffusion equations. Instead of a uniform mesh configuration, a more refined mesh configuration was used in the vicinity of the posts, sharp corners, and along the intersection to insure the accuracy of the calculation. Finite element analysis was applied in a triangular mesh of around 400 000 elements and 200 000 nodal points. It was observed that such a refined mesh configuration was sufficient to provide electric field values which are independent of the number of elements.

Table 4.1 The ranges of some parameters in the simulations

parameter	value	unit
voltage applied on the inlet electrode, ψ_{in}	20	V
voltage applied on the outlet electrode, ψ_{out}	-20	V
diameter of the posts, *d*	(100, 200)	µm
spacing between the posts, *a*	(100, 200)	µm
particle radius, *r*	(0.01 - 10)	µm
zeta potential of the particle, ζ	(0.01 – 1000)	µV
medium relative permittivity, ε_r	(5 – 60)	-

Because of the huge number of mesh elements and in order to make the program run faster, the interpolation function was employed to import the obtained values of the field and field gradients into the convection diffusion module. The ranges of the parameters employed in our simulations are presented in Table 4.1.

4.4 Results and Discussion

The exact solution of local electric field in post array structure coupled with convection-diffusion–migration equation have been used to define the migration mechanism of particles through microfabricated arrays of posts (MFAP) geometry. Using the finite element method, it was possible to conduct a systematic parametric study to define a range of parameters affecting the response of the particles to the applied electric field, such as particle size, permittivity of the medium, and zeta potential of the particles.

In order to emphasize the importance of considering all the migration mechanisms during particle transport in a stationary medium through MFAP geometry two scenarios were considered and shown in Figure 4.3. Figure 4.3 (a) and (b) show the concentration profile while particles are flowing through the post arrays, and Figure 4.3 (c) and (d) present the profile configuration after the particles passed the post array. In what follows, in order to be more precise in our evaluations, all concentration profiles were obtained at the same distance of 1.5 mm from the end of the post array. Figure 4.3 (a) and (c) are obtained with the assumption that the only external force on the particles is electrophoresis, while Figure 4.3 (b) and (d) are obtained with the assumption that the external forces on the particles are electrophoresis and dielectrophoresis. Although the relative magnitude of DEP force to EP force here is very small (around 0.01), one can observe that the concentration profile has been significantly influenced by the presence of dielectrophoresis, as well as the maximum particle concentration in the profile. This implies the importance of considering dielectrophoresis as a defining transport mechanism that can change the fate of particles in post array geometry. The concentration profile of the particles around the posts resulted from dielectr-

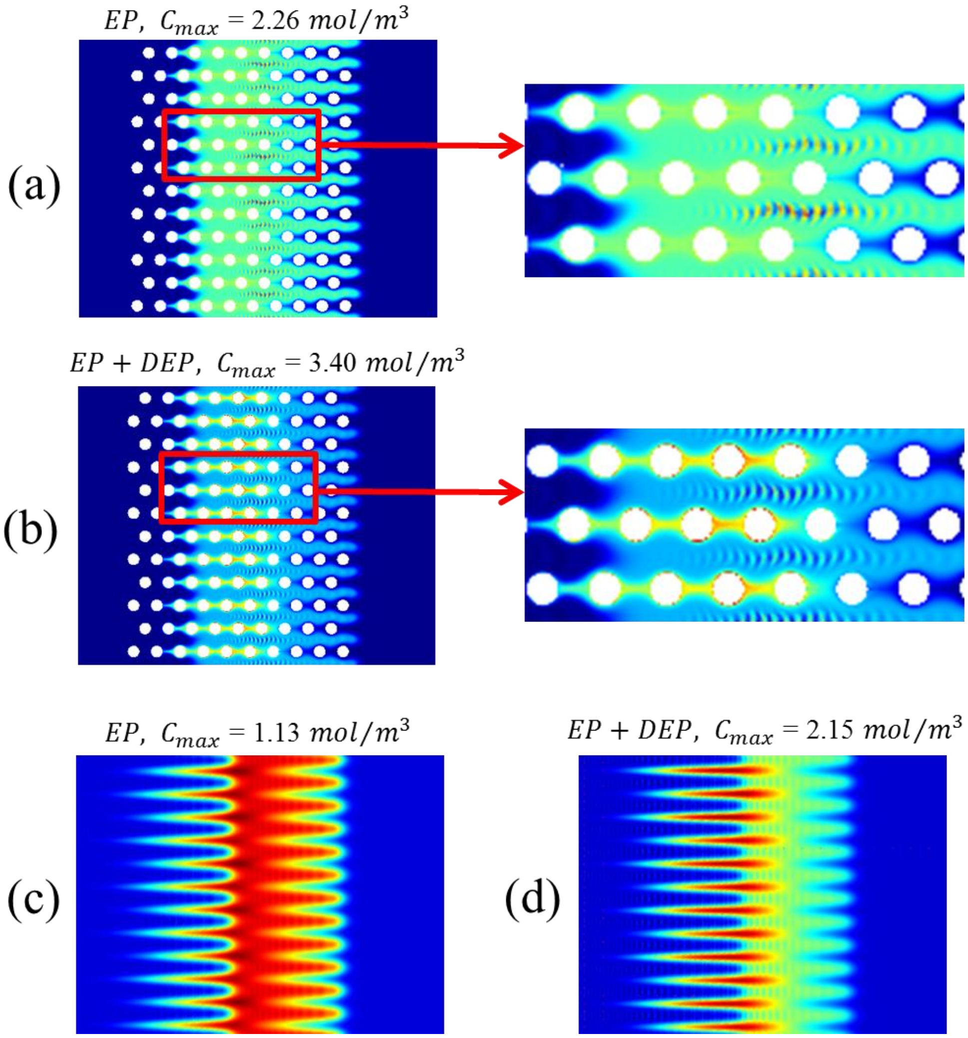

Figure 4.3 Schematic illustrates the effect of DEP on configuration of particles concentration profile. The relative magnitude of DEP to EP forces is around 0.01 and the particle size, medium permittivity and zeta potential of the particles are r = 5μm, ε_r = 1, and ζ = 1mV. (a) and (b) show the concentration profile while particles are passing through the posts (a) ignoring DEP effect, (b) considering DEP. (c) and (d) presents the configuration of the concentration profile after passing the post array (c) ignoring DEP, (d) considering DEP. The significant change in the concentration profile, due to adding DEP effect, reveals the necessity of considering DEP as an effective mechanism in particles transport within the microfabricated devices.

-ophoretic effects (Figure 4.3 d) also implies the ability of dielectrophoresis to separate and concentrate micro/nanoparticles using microfabricated arrays which have been used extensively for cell sorting and handling [30-35].

The relative role of the contributions from convection and diffusion is usually determined by the value of the so-called Peclet number $Pe = rU/D$, where r is the particle radius, U is the relative velocity of a particle with respect to the liquid, and D is the diffusion coefficient of the particle.

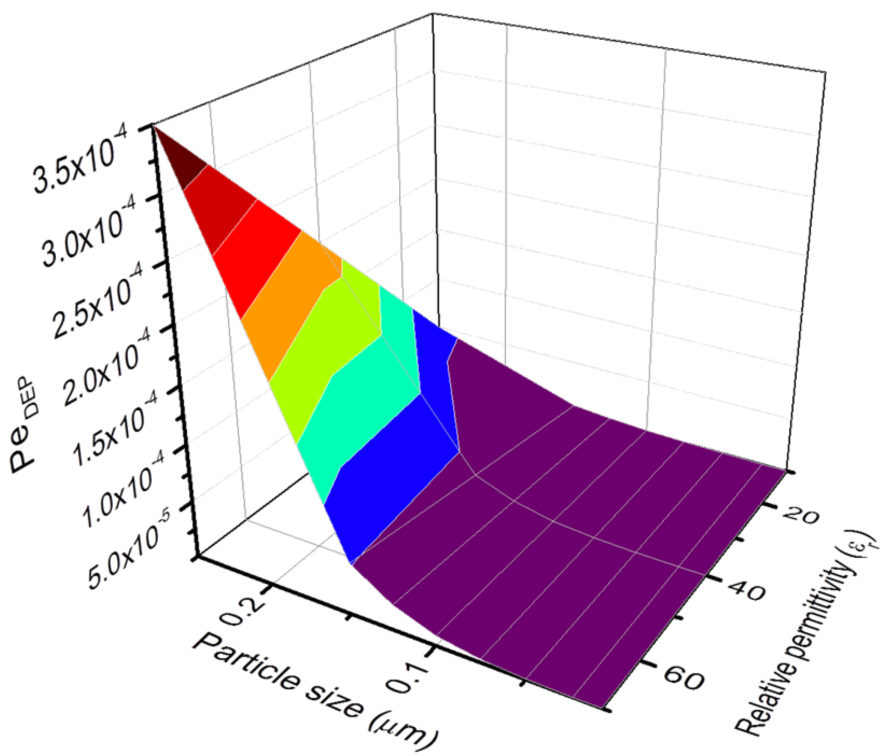

Figure 4.4 Assuming different values of particle size and medium permittivity provided a critical value for Pe_{DEP} above which the dielectrophoresis effect overcomes the diffusion effects in shaping the particle concentration profiles. This critical value for the geometry studied in this work, which is a typical design of a microchannel containing an array of posts, was 10^{-6}. For $Pe_{DEP} > 10^{-6}$ dielectrophoresis dominates diffusion and the DEP induced trapping of particles was observed. Figure 4.5 illustrates the particles trapped around the posts when $Pe_{DEP} > 10^{-6}$.

Figure 4.4 shows the Peclet number based on the characteristic dielectrophoretic velocity (U_{DEP}) as a function of the particle size (radius of the spherical particles) and permittivity of the electrolyte solution. According to this figure, an increment in particle size produces greater Pe_{DEP} based on the dielectrophoretic velocity, i.e., by increasing the particle size dielectrophoresis contribution in particle transport becomes larger compared to diffusion; also increasing the relative permittivity of the medium increases Pe_{DEP}.

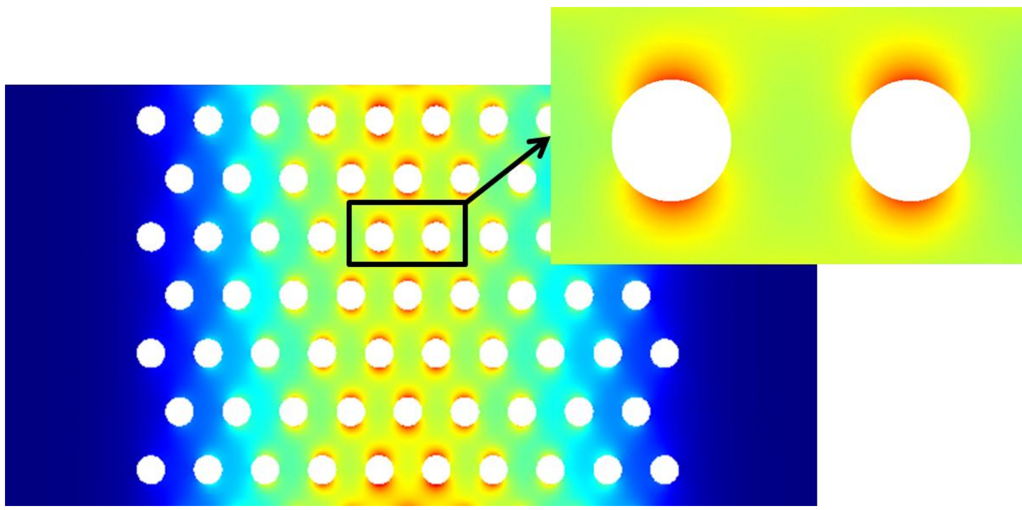

Figure 4.5 Schematic presentation of the particle concentration when $Pe_{DEP} > 10^{-6}$. Dielectrophoresis overcomes diffusion and the particles are concentrated and trapped around the posts where the higher values of the field gradients are present.

Assuming different values of particle size and medium permittivity provided a critical value for Pe_{DEP} above which the dielectrophoresis effect overcomes the diffusion effects in shaping the particle concentration profiles. This critical value for the geometry studied in this work, which is a typical design of a microchannel containing an array of posts, was 10^{-6}. For $Pe_{DEP} > 10^{-6}$ dielectrophoresis dominates diffusion and the DEP induced trapping of particles was observed. Figure 5 illustrate the particles trapped around the posts when $Pe_{DEP} > 10^{-6}$.

Charged particles subjected to a nonuniform electric field also experience electrophoretic forces generally result from the hydrodynamic frictional forces balancing electric field forces. Simulations were conducted to obtain the operating conditions, in form of particle and medium properties, under which the dielectrophoretic effect dominates the electrophoretic effect. The results are presented as variation of the relative value of the Peclet numbers associated with EP and DEP velocities, $Pe_{EP}/Pe_{DEP,}$ with respect to particle and medium properties. Figure 4.6 plots the Pe_{EP}/Pe_{DEP} ratio with respect to zeta potential of the particles. The values of the particle size and medium permittivity were kept constant and equal to 0.25µm and 70, respectively. According to our simulations, for the zeta potentials less than or around 1µV, where the corresponding value of Pe_{EP}/Pe_{DEP} ratio is about 3, DEP dominates EP and the particles are trapped by the posts due to the presence of high field gradients in the vicinity of the posts.

Further simulations were conducted to investigate the dependence of the transport mechanism on the particle size. The post diameter and post-to-post spacing values employed in this evaluation were 200µm and 50µm, respectively. Figure 4.7 illustrates the variation of Pe_{EP}, Pe_{DEP} and Pe_{EP}/Pe_{DEP} with respect to the particle radius based on the simulation results. It can be observed from the figure that Pe_{DEP} increases faster with the particle size compared to Pe_{EP}, therefore Pe_{EP}/Pe_{DEP} decreases by increasing the particle size as shown in Figure 4.7. The values of particle zeta potential and medium permittivity employed here were 0.1mV and 10, respectively. We conducted these calculations in different geometries with different values of post size and post-to-post spacing. We observed that the value of Pe_{EP}/Pe_{DEP} where dielectrophoresis overcomes electrophoresis and particles trapping occurs is constant and equal to 3 regardless of the post size and arrangement.

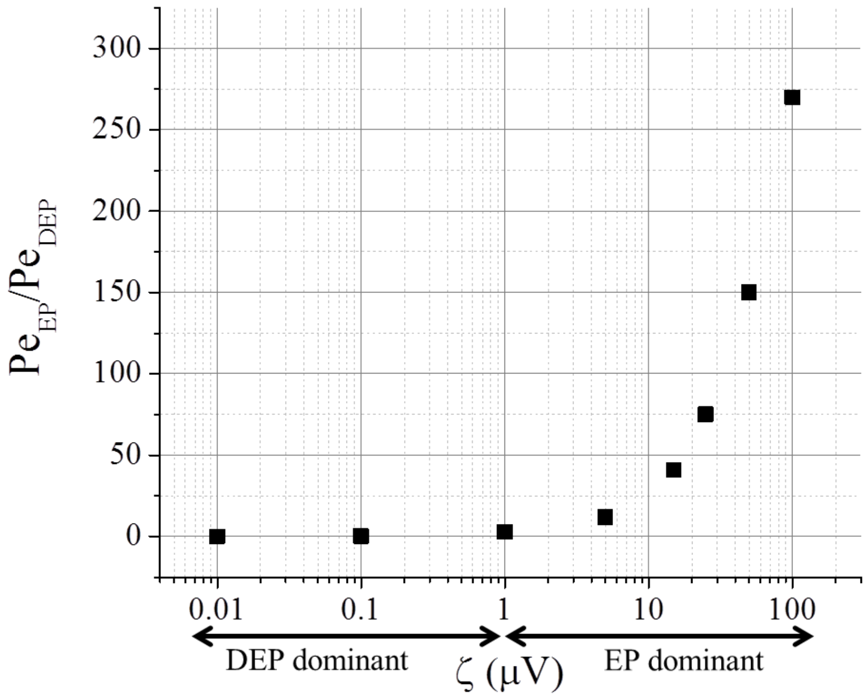

Figure 4.6 Relative value of the Peclet numbers besed on EP and DEP (Pe_{EP}/Pe_{DEP}) vs. zeta potential of the particles. For the values of zeta potential less than 1 μV, DEP dominates EP. The corresponding value of Pe_{EP}/Pe_{DEP} at this point is around 3.

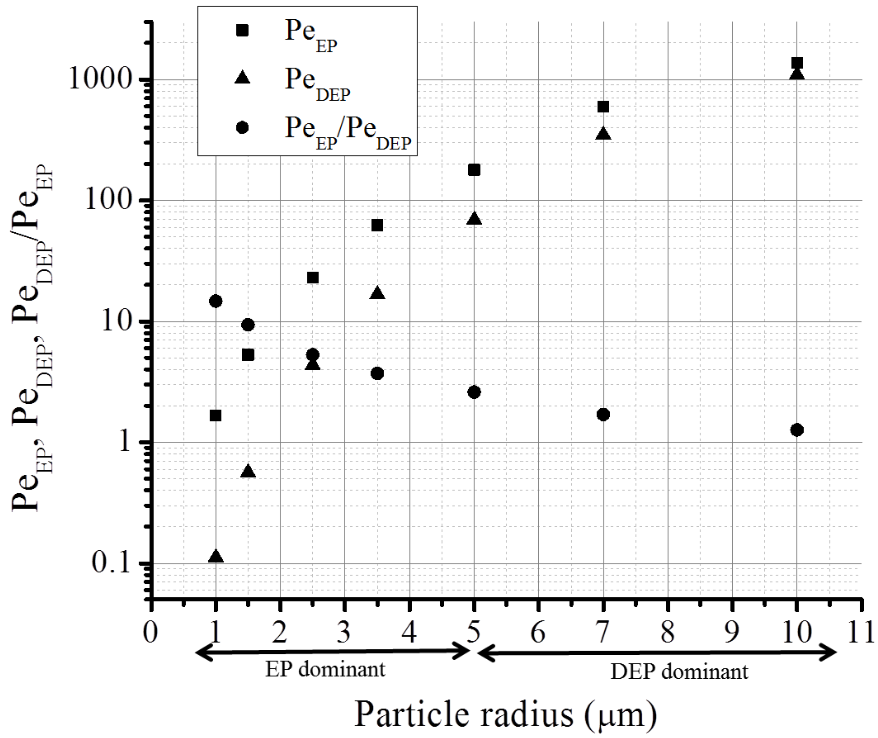

Figure 4.7 Variation of electrophoresis Peclet number (Pe_{EP}), dielectrophoresis Peclet number (Pe_{DEP}) and their ratio (Pe_{EP}/Pe_{DEP}) with respect to the particle radius based on the simulation results. For the particle sizes larger than 5 µm radius, where Pe_{EP}/Pe_{DEP} ratio is around 3, DEP overcomes EP and particles are trapped in the post array.

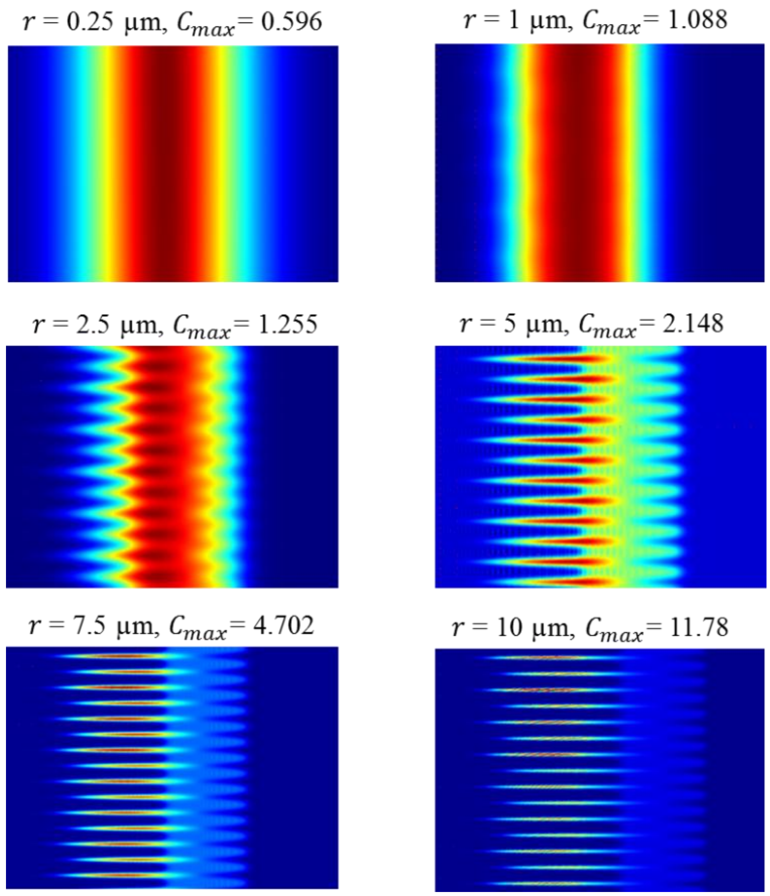

Figure 4.8 Schematic illustration of concentration profile configuration for different particle sizes after passing through the post array. By increasing the particle size, and consequently the Pe_{DEP}/Pe_{EP} ratio, the concentration profile renders to discrete and more concentrated regions.

In order to quantify the effects of different parameters on particle concentration profile, we calculated the band broadening of the concentration profiles once the particles pass through the post arrays. For a normal distribution the band broadening is usually measured by the standard deviation [36, 37]. Since the concentration profiles obtained in this study were not normally distributed, the semi interquartile range which is often used with skewed data [38, 39] was employed instead of standard deviation to measure the band broadening.

The influence of particle size and medium permittivity on band broadening is shown in Figure 4.10 and Figure 4.12. Figure 4.8 illustrates the configuration of concentration profile for different particle sizes after passing through the post array. The same post array as Figure 4.2 was used in the simulations here. All parameters other than the particle size were kept constant; zeta potential of 1mV and medium permittivity of 10 were considered. It was observed in Figure 4.7 that by increasing the particle size, dielectrophoretic force is more dominant compared to electrophoretic force. The results in Figure 4.8 demonstrate the same trend, which as the particle radius increased the concentration profile has been changed from a uniform configuration to some discrete regions due to the presence of high dielectrophoretic forces. It can also be seen that increasing the particle size (higher relative values of DEP force to EP force) results in more concentrated profiles with higher values of maximum concentration, C_{max}, in each profile. This variation is plotted in Figure 4.9. As we can see the higher ratio of Pe_{DEP}/Pe_{EP} provides higher maximum concentrations and renders the profile into more concentrated regions.

The influence of particle size on band broadening of the concentration profile was studied as well. Figure 4.10 presents the relation between the band broadening and particle size. Our results in Figure 4.10 shows that by increasing the particle size, the band broadening increases first, reaches its maximum value at particle radius of 1µm, and then decreases.

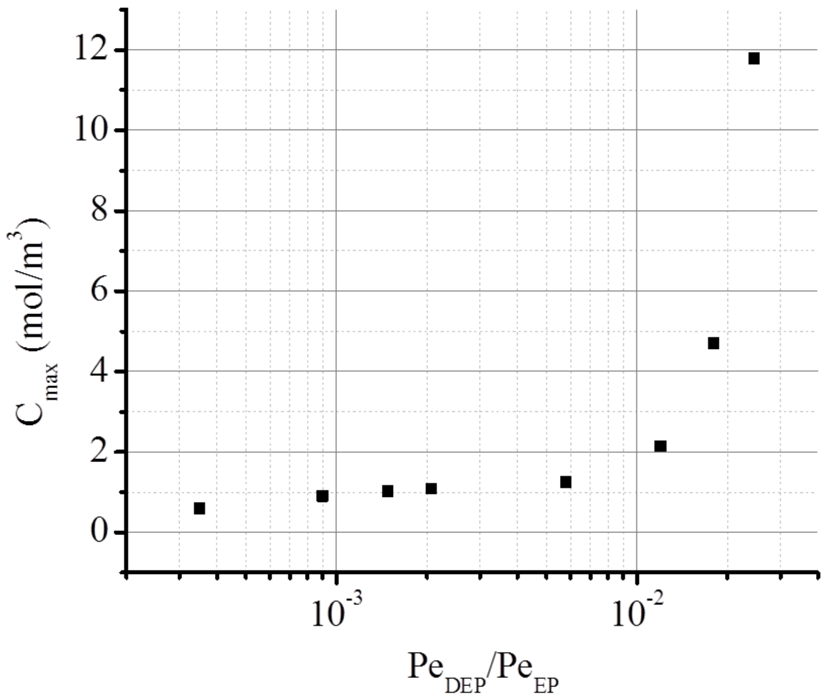

Figure 4.9 Maximum concentration of particles in each profile as a function of Pe_{DEP}/Pe_{EP} ratio. By increasing Pe_{DEP}/Pe_{EP} ratio, the maximum concentration increases, demonstrates the ability of DEP to provide high concentrated profiles.

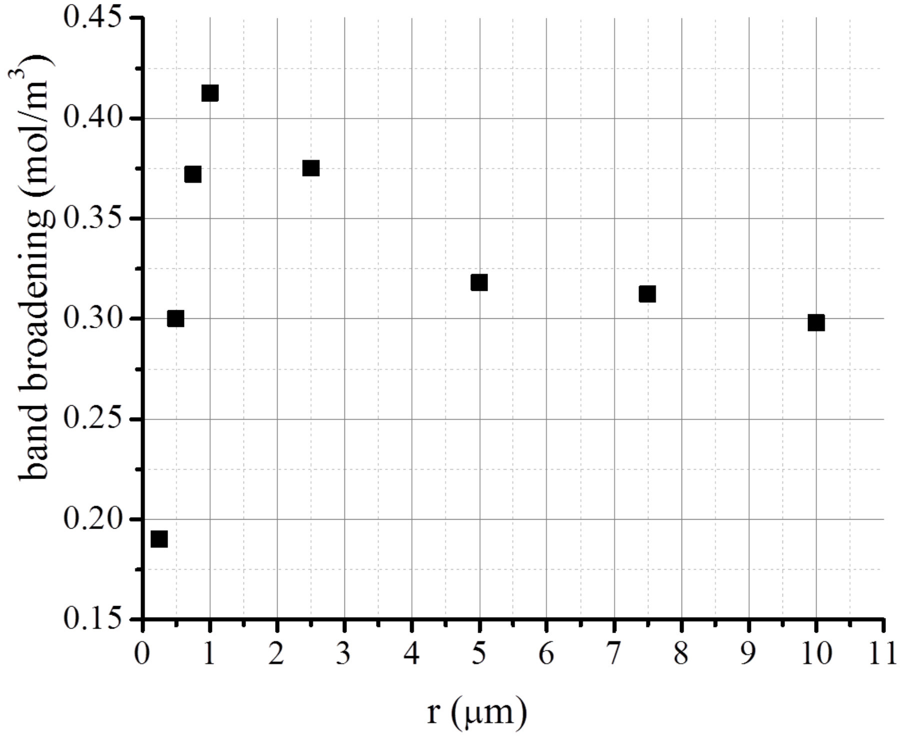

Figure 4.10 Relation between the band broadening and particle size based on the simulation results. The maximum band broadening obtained for particle radius of 1 µm. For particle radius less than one micron, the band broadening increases by increasing the particle size. Conversely, for particle radius of larger than one micron, the band broadening decreases by the particle size.

Effect of medium permittivity on the concentration profile was also evaluated. Figure 4.11 presents the concentration profile of particles after passing the post array for three different values of medium permittivity. The same geometry as Figure 4.2 was used for the simulations, the particle radius of 0.5µm and zeta potential of 1mV were considered. One can see that the medium permittivity affects the particle concentration profiles as well but the effect is not as significant as particle size. From Figure 4.11 we can observe that the value of maximum concentration in each profile does not change significantly with the medium permittivity. Formerly it was observed that by increasing Pe_{DEP}/Pe_{EP} ratio, higher values of C_{max} were obtained. We calculated Pe_{DEP}/Pe_{EP} for different values of medium permittivity and observed that Pe_{DEP}/Pe_{EP} does not change significantly and assume a value around 9×10^{-4}. This observation shows that changing the medium permittivity does not change the maximum concentration, C_{max}, as significantly as changing the particle size.

The effect of medium permittivity on band broadening of the concentration profile was also evaluated and the result is presented in Figure 4.12. The values of zeta potential and particle radius were kept constant and equal to 1mV and 0.5µm, respectively. This figure demonstrates that for a specific particle size, band broadening decreases by increasing the medium permittivity.

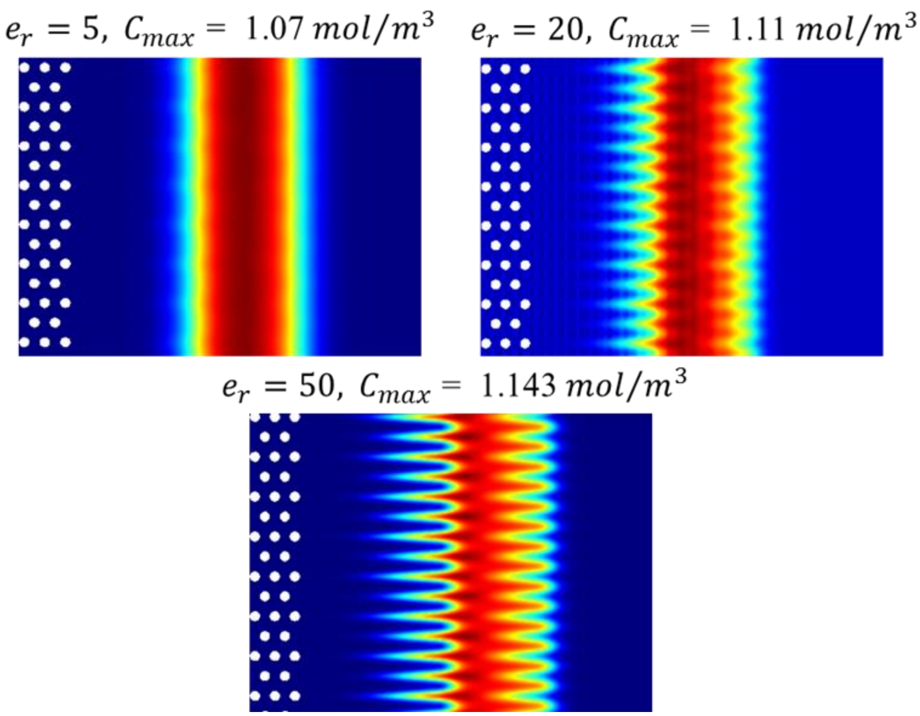

Figure 4.11 Schematic illustration of the concentration profile after passing through the post array for three different medium permittivities. Medium permittivity cannot affect the value of maximum concentration significantly, since the Pe_{DEP}/Pe_{EP} ratio does not change by medium permittivity. But the profile configuration is influenced by the medium permittivity.

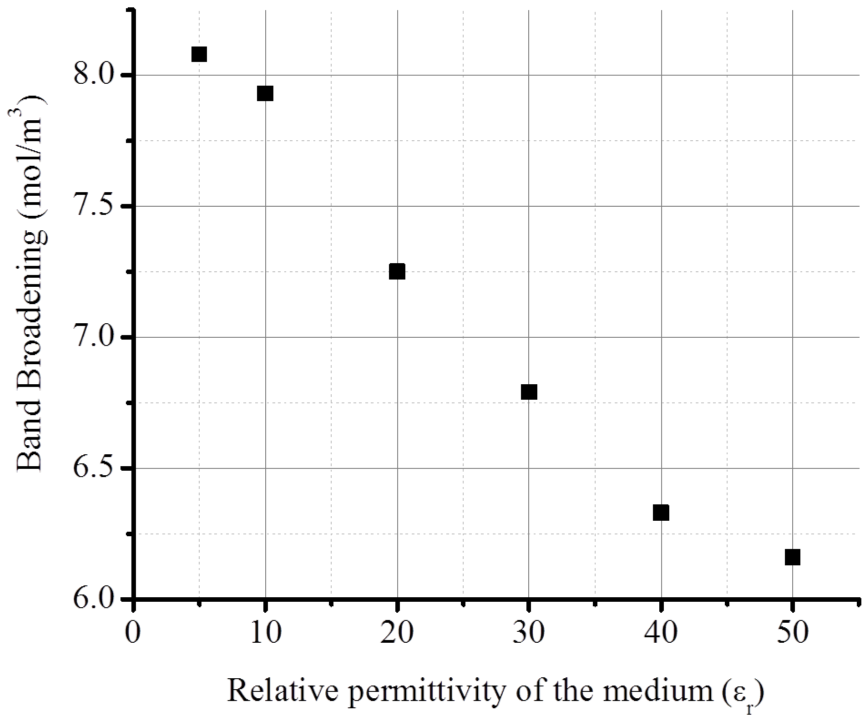

Figure 4.12 Effect of medium permittivity on band broadening of the concentration profile. The band broadening decreases as the medium permittivity increase.

4.5 Conclusion

Microfabricated post arrays (MFPA) have been evaluated in numerous studies [22, 30, 34, 40-44] for various applications including separation, mixing and manipulation of micron scale entities through different electrophoretic and dielectrophoretic techniques. In this study, the fate of particles through uniform arrays of posts was studied in the presence of diffusion, electophoresis, and dieletrophoresis forces. Performing numerical simulations using finite element method, we tried to introduce a criteria based on the particles and medium properties and magnitude of the applied field, where one of the mentioned mechanisms, i.e., DEP, EP, or D is the governing mechanism in defining the particle concentration profiles. The results are presented in form of Peclet number which shows the relative role of the contributions from convection and diffusion. It was obtain that when Pe_{DEP}, which is the Peclet number based on dielectrophoretic motion of the particles, is larger than 10^{-6}, dielectrophoresis overcomes diffusion resulting in particles trapping around the posts where high electric field gradients are present within the MFPA. Our simulations also explored a critical value for the relative magnitude of the electrophoretic and dielectrophoretic forces, in form of Pe_{EP}/Pe_{DEP}, under which the dielectrophoresis dominates electrophoresis so that the MFPA has the potential to trap particles. Different post arrays with different post sizes and post-to-post distances were studied and it was observed that around the critical value of $Pe_{EP}/Pe_{DEP} = 3$, the particle trapping occurs independent of MFPA geometry. Further simulations were conducted to understand the influence of the particle size and medium permittivity on the particles concentration profile. It was observed that by increasing the particle size, and consequently the relative magnitude of the DEP force to electrophoretic force, the configuration of the concentration profile rendered to some discrete and more concentrated regions. The effect of particle size on band broadening of the concentration profile was also evaluated and it was observed that for the particle sizes of smaller than 1 µm, the band broadening increases by the particle size. Conversely, for particles larger than 1 µm, increasing the particle size causes more band broadenings. Therefore, the maximum band broadening of the concentration profile is present for the particle size of 1 µm. The investigation on the effect of medium permittivity on the concentration profile revealed that although this parameter changes the configuration of the profile; it cannot produce significantly higher C_{max}. Furthermore, it was observed that by increasing the medium permittivity the band broadening of the concentration profile increases monotonously.

The results obtained in this study have the potential to be used in designing the electrophoretic and dielectrophoretic-based separation and concentration processes by showing how the properties of the medium and particle and the relative magnitude of the EP and DEP forces can change the particle fate in MFPA geometries.

References

[1] Velev, O. D., Bhatt, K. H. *Soft Matter* 2006, *2*, 738-750.

[2] Andersson, H., van den Berg, A. *Sensors and Actuators B-Chemical* 2003, *92*, 315-325.

[3] Escarpa, A., Cristina Gonzalez, M., Lopez Gil, M. A., et al. *Electrophoresis* 2008, *29*, 4852-4861.

[4] Chung, T. D., Kim, H. C. *Electrophoresis* 2007, *28*, 4511-4520.

[5] Dittrich, P. S., Tachikawa, K., Manz, A. *Analytical Chemistry* 2006, *78*, 3887-3907.

[6] Rhee, M., Burns, M. A. *Lab on a Chip* 2008, *8*, 1365-1373.

[7] Martinez-Lopez, J. I., Moncada-Hernandez, H., Baylon-Cardiel, J. L., et al. *Analytical and Bioanalytical Chemistry* 2009, *394*, 293-302.

[8] Pohl, H. A. *Journal of applied Physics* 1951, *22*, 869-871.

[9] Pohl, H. A. *Dielectrophoresis*, Cambridge University Press: Cambridge 1978.

[10] Pethig, R. *Crit. Rev. Biotechnol.* 1996, *16*, 331-348.

[11] Ramos, A., Morgan, H., Green, N. G. *Appl. Phys.* 1998, *31*, 2338-2353.

[12] Jones, T. B. ***Electromechanics of Particles***, Cambridge University Press: New York 1995.

[13] Pysher, M. D., Hayes, M. A. *Analytical Chemistry* 2007, *79*, 4552-4557.

[14] Morgan, H., Green, N. G. *AC Electrokinetics: Colloids and Nanoparticles*, Research Studies Pr 2003.

[15] Castellanos, A., Ramos, A., Gonzalez, A., et al. *Journal of Physics D-Applied Physics* 2003, *36*, 2584-2597.

[16] Chou, C. F., Zenhausern, F. *IEEE Engineering in Medicine and Biology Magazine* 2003, *22*, 62-67.

[17] Chou, C. F., Tegenfeldt, J. O., Bakajin, O., et al. *Biophysical Journal* 2002, *83*, 2170-2179.

[18] Sabounchi, P., Morales, A. M., Ponce, P., et al. *Biomedical Microdevices* 2008, *10*, 661-670.

[19] Jeon, W., Shin, C. B. *Chemical Engineering Journal* 2009, *152*, 575-582.

[20] Moncada-Hernandez, H., Baylon-Cardiel, J. L., Perez-Gonzalez, V. H., et al. *Electrophoresis* 2011, *32*, 2502-2511.

[21] Cummings, E. B. *IEEE Engineering in Medicine and Biology Magazine* 2003, *22*, 75-84.

[22] Cummings, E. B., Singh, A. K. *Analytical Chemistry* 2003, *75*, 4724-4731.

[23] Nakano, A., Camacho-Alanis, F., Chao, T., et al. *Biomicrofluidics* 2012, *6*, 034108.

[24] Xu, Y. C., Vaidya, B., Patel, A. B., et al. *Analytical Chemistry* 2003, *75*, 2975-2984.

[25] Shiu, J., Whang, W., Chen, P. *Journal of Chromatography a* 2008, *1206*, 72-76.

[26] Kuo, C., Shiu, J., Wei, K. H., et al. *Journal of Chromatography a* 2007, *1162*, 175-179.

[27] Chen, G. D., Fachin, F., Fernandez-Suarez, M., Wardle, B. L., Toner, M. *Small* 2011, *7*, 1061-1067.

[28] De Pra, M., Kok, W. T., Schoenmakers, P. J. *Journal of Chromatography a* 2008, *1184*, 560-572.

[29] Masliyah, J. H., Bhattacharjee, S. *Electrokinetic and colloid transport phenomena*, Wiley 2006.

[30] Castelino, J., Austin, R. *Biophys. J.* 2000, *78*, 254A-254A.

[31] Chou, C., Austin, R., Bakajin, O., Tegenfeldt, J. *et al*. *Electrophoresis* 2000, *21*, 81-90.

[32] Bakajin, O., Duke, T., Chou, C., Tegenfeldt, J. *et al*. *Biological Physics* 1999, *487*, 243-248.

[33] Moraes, C., Chen, J., Sun, Y., Simmons, C. A. *Lab on a Chip* 2010, *10*, 227-234.

[34] Hunt, T., Lee, H., Westervelt, R. *Appl. Phys. Lett.* 2004, *85*, 6421-6423.

[35] Wei, C., Huang, J., Lu, C., Han, W. *et al*. *The study of microfluidic chip with micro cylindrical post array for separating particles* 2007.

[36] Berthod, A. *Journal of Chromatography a* 2006, *1126*, 347-356.

[37] Busnel, J., Foucault, F., Denis, L., Lee, W., Chang, T. *Journal of Chromatography a* 2001, *930*, 61-71.

[38] http://srmo.sagepub.com/view/encyclopedia-of-measurement-and-statistics/n403.xml

[39] http://www.google.ca/url?sa=t&rct=j&q=&esrc=s&source=web&cd=5&cad=rja&ved=0CEoQFjAE&url=http%3A%2F%2Facademic.udayton.edu%2Fgregelvers%2Fpsy216%2Fppt%2Fdispersion.ppt&ei=HMHwUOm4Aq6PigLo5IDACQ&usg=AFQjCNFlx2giY4vnTYTWLP7L6jqa2nC5jQ&sig2=Az8E-at4XN_QFJLN4v7ycw&bvm=bv.1357700187

[40] Lapizco-Encinas, B., Simmons, B., Cummings, E., Fintschenko, Y. *Anal. Chem.* 2004, *76*, 1571-1579.

[41] Huang, L., Tegenfeldt, J., Kraeft, J., Sturm, J. *et al*. *Nat. Biotechnol.* 2002, *20*, 1048-1051.

[42] Ou, J., Joswiak, M. N., Carpenter, S. J., Dorfman, K. D. *Journal of Vacuum Science & Technology a* 2011, *29*.

[43] Bhattacharya, S., Chao, T., Ros, A. *Electrophoresis* 2011, *32*, 2550-2558.

[44] Zeng, Y., He, M., Harrison, D. J. *Angewandte Chemie-International Edition* 2008, *47*, 6388-6391.

5 Conclusion and Future Work

5.1 Concluding Remarks

The parametric study performed in this work provides guidelines for designing the electrokinetic processes, including the electrophoretic and dielectrophoretic-based separation and concentration processes in MFPAs. Based on the literature review, numerous publications were found that focus on the study of microfabricated structures, especially MFPAs, for purposes such as particle manipulation, separation, and concentration. However, there was a lack of characteristic study of MFPAs in order to systematically design the processes, which is required to proper use of these microfabricated structures. It was shown in this work that the geometry of MFPAs can be employed to produce the desired electric field and field gradients required for each process, through the posts' shape, size, surface-to-surface distance, and arrangement. As well the relative magnitude of the contributions from diffusion, electrophoresis and dielectrophoresis within the MFPAs, was introduced as a measure to determine the dominant mechanism for the particle transport in these devices.

The major conclusions that can be drawn from this parametric study of microfabricated structures are summarized below:

1. For the microchip geometry with no post array, our results provided criteria where the assumption of uniform field is valid, which can have important implications in designing microfluidic units where a high field gradient is either favored (mixing) or not favored (separation). It was observed that in the vicinity of the junction between the chamber and microchannels, the field orientation significantly deviated from its nominal values. We defined a "safe zone" in the chamber where the deviation of the field orientation from its nominal value was less than 5%.

Our calculations showed that the dimension of this zone was affected by the chamber size, channels surface charge, and the difference between the voltages applied at the injection channel and side channels.

2. The electric field and field gradients were also calculated in a MFPA. The magnitude of the electric field was monotonously increased by the diameter over the post-to-post spacing (d/a) ratio, while the field gradients were increased by d/a multiplied by the total number of the posts in the array. The highest values of the field and field gradients were obtained for the structures with rectangular posts, where their diagonals were in the direction of the field orientation.

3. The effect of array arrangement on the field gradients was observed to depend on the diameter over the post-to-post spacing (d/a) ratio. For $d/a < 1$, the square arrangement provided larger values of the field gradients, whereas for $d/a > 1$, the hexagonal arrangement yielded larger field gradients. For $d/a = 1$, both arrangements exhibited the equal values of the field gradients.

4. The DC dielectrophoretic and electrophoretic effects on the concentration of particles through uniformly patterned arrays of posts were also evaluated. The results were presented in form of the Peclet number, which shows the relative role of the contributions from convection and diffusion. It was found that when Pe_{DEP}, which is the Peclet number based on the dielectrophoretic motion of the particles, was larger than 10^{-6}, dielectrophoresis overcame diffusion, resulting in the particles being trapped within the MFPA to occur.

5. A critical value for the relative magnitude of the electrophoretic and dielectrophoretic forces exerted on the particle in a MFPA was introduced in form of the Pe_{EP}/Pe_{DEP} ratio, under which the dielectrophoresis dominated electrophoresis so that the MFPA had the potential to trap particles. This critical value, which was observed to be independent of the post array geometry, was around 3 ($Pe_{EP}/Pe_{DEP} = 3$).

6. Our investigation of the effect of particle size and medium permittivity on the concentration profile in a MFPA found that for the particle sizes smaller than 1 µm, the band broadening increased by the particle size. Conversely, for particles larger than 1 µm, increasing the particle size caused more band broadenings. Therefore, the maximum band broadening of the concentration profile was present for the particles of 1 µm. It was also found that the band broadening was decreased by increasing the medium permittivity.

5.2 Future Works

The study presented here should be considered as the initial step in a thorough investigation of the characterization of the microfabricated post arrays and the electrokinetic based processes within these microstructures. Some simplifications were made during this study that may not be suitable for a more general investigation. Some of the significant recommendations that can be made to achieve a more rigorous investigation are listed below:

1. According to our results, different post array arrangements with the same post diameter and surface-to-surface distance provided different values for the field gradients. In this study, only two typical arrangements for the post array were evaluated. In order to perform a more comprehensive study, other arrangements, e.g., random structures, can be investigated to

determine the arrangement which produces the highest field gradients required for dielectrophoretic based processes.

2. When a DC electric field is applied through the microchannel, the electrokinetic velocity comprises the effects of electrophoresis and electroosmosis. In this study, the electroosmotic velocity of the particles was assumed to be small and near zero, since the assumption of a high concentrated electrolyte and very small zeta potential of the microchannel was made. Therefore, the model used to evaluate the electrokinetic forces in this study should be modified to account for the electroosmosis effect, which is significant in many cases.

3. In this study, the particles were assumed to be more polarizable than the medium which caused the positive dielectrophoresis to occur. In a DC field, this assumption is valid when the particle has higher conductivity than that of the medium. The evaluation of the opposite case, i.e., negative dielectrophoresis, may lead to the introduction of other criteria for the particle transport mechanism in the microfabricated post arrays.

4. The electrophoretic force was calculated by employing the Helmholtz-Smoluchowski equation, which is valid when the Debye screening length is small relative to the particle radius ($\kappa a >> 1$), i.e., the double layer is extremely thin compared to the particle radius. A more rigorous approach towards calculating the electrophoretic force can be achieved by using Henry's equation, which is valid for all κa values.

5. Finally, by using microlithographic techniques, an experimental investigation can be performed to evaluate the consistency of the simulation results and the experimental measurements.

Appendix A

Agreement between analytical solution and COMSOL Multiphysics solution

The following problem was solved analytically and simulated by using COMSOL Multiphysics. The comparison of the results showed that the simulation results agreed with the analytical results.

Two-dimensional dielectric slab in external electric field

A flat polymer slab of permittivity ε_2 and thickness 2d is located in a dielectric medium of permittivity ε_1. The potential at x= -X is Ψ_A and at x=X is Ψ_B. The geometry is shown in Figure A.1.

Analytical Solution

The medium and the slab, which are dielectric materials, have no free charges, so the governing equation is the Laplace equation

$$\nabla^2\Psi = 0$$

In this case, the geometry is one dimensional and Laplace's equation must be written in one dimension

$$\partial^2\Psi/\partial x^2 = 0$$

This equation is applicable to all three regions.

The solution is

$$\Psi_1 = a_1+b_1x \qquad -X \leq x \leq -d$$

$$\Psi_2 = a_2+b_2x \qquad -d\leq x \leq d$$

$$\Psi_3 = a_3+b_3x \qquad d\leq x \leq X$$

The Boundary conditions are

$\Psi_1 = \Psi_A$ x = -X (Imposed potential)

$\varepsilon_1 \frac{d\Psi 1}{dx} = \varepsilon_2 \frac{d\Psi 2}{dx}$ x = -d (No surface charge)

$\Psi_1 = \Psi_2$ x = -d (Continuity of potential)

$\Psi_2 = \Psi_3$ x = d (Continuity of potential)

$\varepsilon_2 \frac{d\Psi 2}{dx} = \varepsilon_1 \frac{d\Psi 3}{dx}$ x = d (No surface free charge)

$\Psi_3 = \Psi_B$ x = X (Imposed potential)

Applying the boundary conditions above, one can obtain

$\Psi_1 = (\Psi_A+ \Psi_B)/2 – C\ d\ (\varepsilon_2- \varepsilon_1)\ (\Psi_A- \Psi_B) – C\ \varepsilon_2\ (\Psi_A- \Psi_B)\ x$

$\Psi_2 = (\Psi_A+ \Psi_B)/2 – C\ \varepsilon_1\ (\Psi_A- \Psi_B)\ x$

$\Psi_3 = (\Psi_A+ \Psi_B)/2 + C\ d\ (\varepsilon_2- \varepsilon_1)\ (\Psi_A- \Psi_B) – C\ \varepsilon_2\ (\Psi_A- \Psi_B)\ x$

$C = 1/\ (2[\varepsilon_2X – d\ (\varepsilon_2- \varepsilon_1)])$

The electric field is defined as

$$E = - \frac{d\Psi}{dx}$$

$$\begin{cases} E_1 = C\ \varepsilon_2\ (\Psi_A- \Psi_B) \\ E_2 = C\ \varepsilon_1\ (\Psi_A- \Psi_B) \\ E_3 = C\ \varepsilon_2\ (\Psi_A- \Psi_B) \end{cases}$$

The values considered for each parameter are shown in Table A.1.

Applying these values, one can obtain

$$C = 0.01009$$

$$\begin{cases} \Psi_1 = 30 - 1.4285 - 10.71558x \\ \Psi_2 = 30 - 3.57186x \\ \Psi_1 = 30 + 1.4285 - 10.71558x \end{cases}$$

$$\begin{cases} E_1 = 10.71558 \\ E_2 = 3.57186 \\ E_3 = 10.71558 \end{cases}$$

COMSOL Multiphysics Solution

Since the system has no free charge, the potential field is obtained by solving Laplace's equation for the potential, $\nabla^2\psi = 0$. The COMSOL Multiphysics implementation is straightforward. The problem is solved by using COMSOL 3.5a, the applied mode is 2D electrostatic, and the mesh size is extra fine and consists of 2310 triangular elements. The geometry is simply modeled by using lines. The zero charge/symmetry condition is applied to all boundaries except where we have imposed the potential, at $x = -X$ and $x = X$, and the electric potential condition is applied to these boundaries. The input data are tabulated in Table A.1. Figures A.2 and A.3 plot the COMSOL Multiphysics solutions for the potential and electric field.

The electric field distribution obtained from the COMSOL Multiphysics solution is

$$\begin{cases} E_1 = 10.714286 \\ E_2 = 3.571429 \\ E_3 = 10.714286 \end{cases}$$

Both the analytical and COMSOL Multiphysics solutions provided the same results.

Table A.1 Values considered for each parameter

ε_1	8.85×10^{-12} ($C^2/N.m^2$)
ε_2	$3\times 8.85 \times 10^{-12}$ ($C^2/N.m^2$)
Ψ_A	50(V)
Ψ_B	10(V)
D	0.2 (m)
X	2 (m)

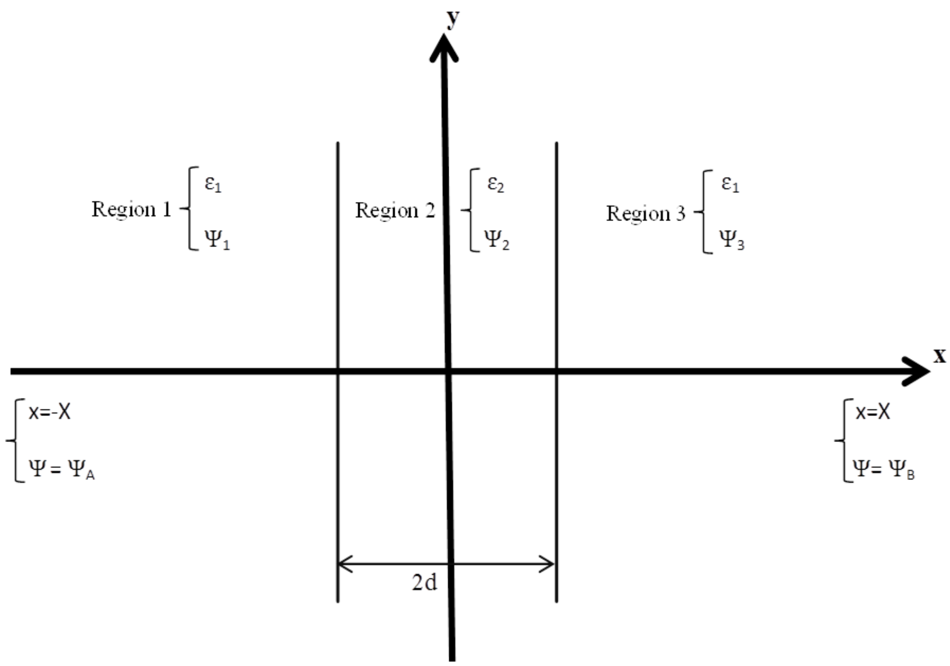

Figure A.1. Polymer slab in a dielectric medium with an imposed electric potential

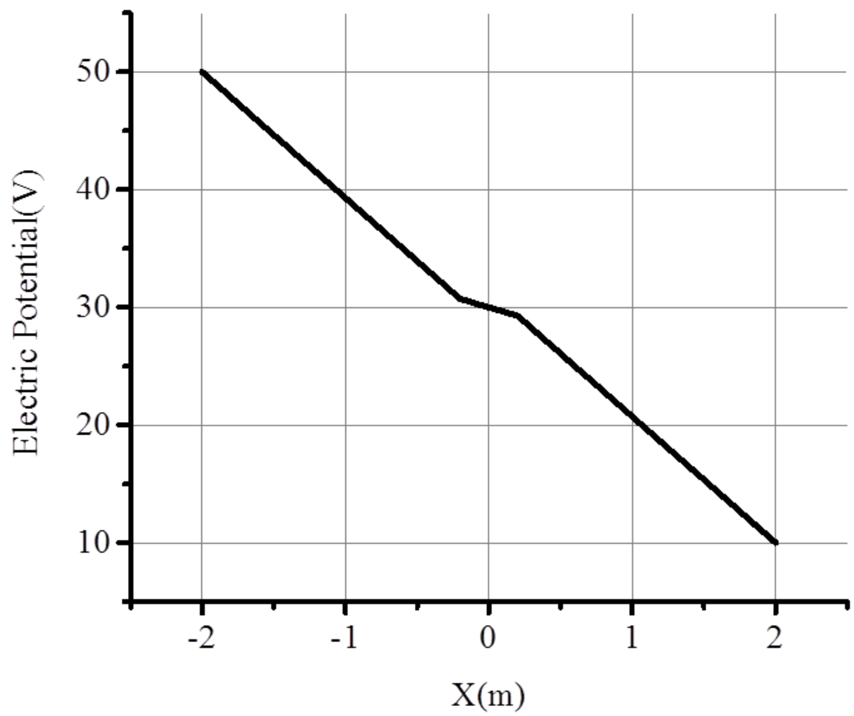

Figure A.2. Electric potential vs. position resulted from simulation by COMSOL Multiphysics

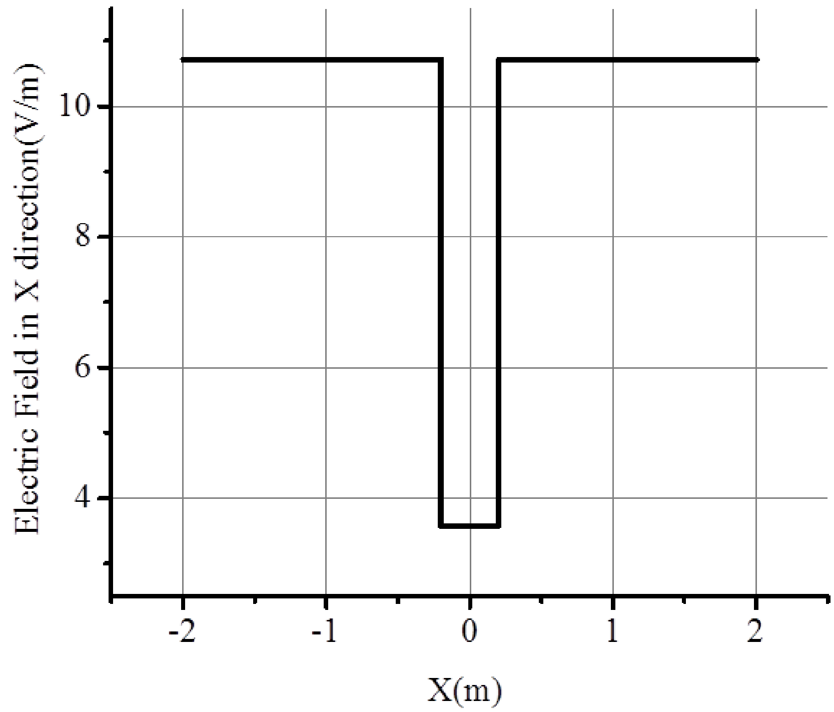

Figure A.3. Electric Field in X direction vs. position obtained from COMSOL Multiphysics solution